Alma Mater Studiorum Università di Bologna
Archivio istituzionale della ricerca

Fault-Tolerant Torque Controller Based on Adaptive Decoupled Multi-Stator Modeling for Multi-Three-Phase Induction Motor Drives

(Article begins on next page)

16 August 2024

Fault-Tolerant Torque Controller Based on Adaptive Decoupled Multi-Stator Modeling for Multi-Three-Phase Induction Motor Drives

Sandro Rubino, Fabio Mandrile, Eric Armando, Radu Bojoi
Dipartimento Energia
"G. Ferraris"
Politecnico di Torino
Torino, Italy
sandro.rubino@polito.it - radu.bojoi@polito.it

Luca Zarri
Dept. of Electrical, Electronic and Information Engineering
"G. Marconi"
University of Bologna
Bologna, Italy
luca.zarri2@unibo.it

Abstract—Among the multiphase solutions, multi-three-phase drives are becoming more and more widespread in practice as they can be modularly supplied by conventional three-phase inverters. The literature reports several control approaches to perform the torque regulation of multi-three-phase machines. Most of such solutions use the vector space decomposition (VSD) approach since it allows the control of a multi-three-phase machine using the conventional control schemes of three-phase drives, thus reducing the complexity of the control algorithm. However, this advantage is practically lost in the case of open-three-phase faults. Indeed, the post-fault operation of the VSD-based drive schemes requires the implementation of additional control modules, often specifically designed for the machine under consideration. Therefore, this paper aims to propose a novel control approach that allows using any control scheme developed for three-phase motors to perform the torque regulation of a multi-three-phase machine both in healthy and faulty operation. In this way, the previously mentioned drawbacks of the VSD-based control schemes in dealing with the faulty operation of the machine are avoided. Moreover, the simplicity of the control algorithm is always preserved, regardless of the machine's operating condition. The proposed solution has been experimentally validated through a 12-phase induction motor, rated 10 kW at 6000 r/min, using a quadruple-three-phase configuration of the stator winding.

Keywords—direct flux vector control, fault-tolerant torque control, induction motor drives, multiphase electrical machines.

I. Introduction

As a result of the current electrification processes of wind energy production and transportation, multiphase solutions are becoming a competitive alternative to the conventional three-phase motor drives [1]–[4]. Indeed, multiphase machines significantly reduce the current levels for a given electric power, making it possible to use today's fast power electronics devices and, hence, getting significant advantages in terms of efficiency and power density [3], [5], [6].

Among the multiphase solutions, multi-three-phase motor drives are experiencing significant interest from the industry because such systems allow configuring a multiphase machine as multiple three-phase units operating in parallel [1]. In this way, several advantages can be obtained. The first advantage is a straightforward machine design since the stator consists of multiple three-phase winding sets having isolated neutral points. The second advantage is that using three-phase inverter power modules reduces cost and design time. Three-phase inverter modules are used to supply each winding set, as shown in Fig. 1. Therefore, the fault-tolerance capability is implemented according to the three-phase modularity [1]. In the case of a fault in a power module, this is turned off, and the corresponding unit, i.e., winding set plus inverter, is disconnected from the dc-link [7], thus getting a straightforward post-fault drive reconfiguration.
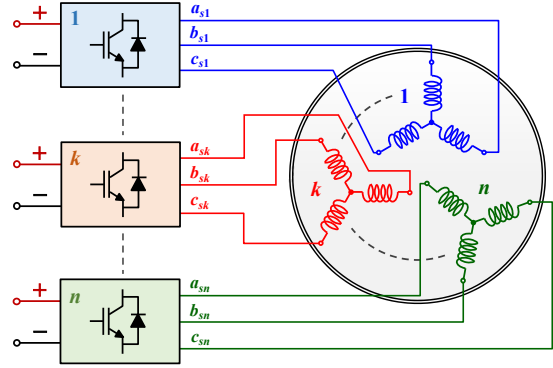

Fig. 1. Multi-three-phase drive topology.

Although a fault event leads to losing an entire winding set, the fault-tolerant strategies based on the three-phase modularity allow the following advantages [2]:

- Each three-phase unit acts as a balanced load on the dc-supply (see Fig. 1) and avoids low-order harmonic content on the dc-link current.
- Each three-phase winding set produces a smooth torque contribution [1], [7]. Therefore, losing one or more three-phase units does not introduce torque ripple or drag torque. The control strategy following a fault is to increase the torque demand for the healthy winding sets, thus compensating for the missing torque contributions of the faulty winding sets.

Finally, the third advantage of multi-three-phase drives is the possibility of implementing power-sharing strategies among the three-phase winding sets [7], [8]. Such strategies help the series-parallel systems [8], [9], i.e., series or parallel connection of the dc-links belonging to the three-phase inverter units. Application examples of such systems can be found in wind energy production [8]. However, it is highlighted that most of the multi-three-phase drives for high-power applications (e.g., oil and gas [10]) usually operate with balanced operation among the units, optimizing the overall machine efficiency [8].

Regardless of the drive operation, most control solutions implemented for multi-three-phase machines are based on the vector space decomposition (VSD) approach [11]. The VSD approach decomposes the multiphase machine model into multiple orthogonal subspaces. The main subspace performs the electromechanical energy conversion if a sinusoidal distribution of the stator windings is considered. Instead, the other subspaces have the meaning of time-harmonic and zero-sequence patterns of the machine [12]. The main advantage of such an approach is evident since, for healthy operation with balanced three-phase units, the torque control scheme should actively manage only the main subspace. Thus, most control schemes developed for three-phase motors can be used [13], e.g., field-oriented control (FOC).

Unfortunately, the VSD can deal only with machines having a symmetrical or asymmetrical configuration of the stator winding [14], [15]. Besides, if an open-three-phase fault occurs, the VSD-based algorithms must actively control the time-harmonic subspaces to keep the machine waveforms (e.g., phase-currents) balanced and within their boundaries. Hence, they require the implementation of specific control modules supported by dedicated fault-tolerant strategies [6], [16]–[19], and both often must be explicitly designed for the machine under consideration.

A viable alternative to the VSD-based control schemes is modular algorithms like those based on the multi-stator (MS) approach [1], [20]. In this case, the machine stator is considered as multiple three-phase winding sets interacting with each other and with an equivalent three-phase rotor. In this way, the flux and torque contributions of each winding set are highlighted. Therefore, the MS approach is suitable for implementing modular control schemes [7], [21], [22] and permits both power-sharing strategies among the units and post-fault machine operation. Unlike the VSD approach, the MS can also deal with stator winding configurations different from the symmetrical or asymmetrical ones [21], [23]. However, the MS-based drive solutions require specific control schemes. Also, specific decoupling algorithms [7], [21] need to be implemented to prevent instability phenomena since the winding sets are magnetically coupled [1], [20], [24].

Recently, some attempts to combine the advantages of the VSD and MS approaches have been proposed [25], [26]. In [27], [28], general solutions that consider a generic number of winding sets have been developed, leading to the definition of the decoupled MS (DMS) approach. According to [27], a DMS-based control scheme is structured like a VSD-based one but keeps the modularity features. Nevertheless, like the VSD-based schemes, the solution proposed in [27] requires implementing additional control modules to perform the post-fault drive operation.

Therefore, this paper proposes a novel control approach that allows the torque regulation of a multi-three-phase machine both in healthy and faulty operating conditions by using any of the conventional control algorithms for three-phase drives. The proposed control approach uses the DMS modeling [27], [28], thus expressing the machine torque production using common- and differential- mode subspaces. Nevertheless, unlike DMS-based control solutions [27], [28], the torque regulation is performed by actively controlling only the common-mode subspace, regardless of the machine's operating condition (healthy or faulty). Therefore, compared to the control solutions based on VSD or DMS reported in the literature, the proposed control approach brings the following advantages and contributions:

1) The drive scheme does not require additional control modules to regulate the machine torque after an open-three-phase fault event. Hence, the simplicity of the control structure is preserved in any operating condition.
2) The control approach can be applied to any multi-three-phase machine configuration, thus overcoming the VSD restrictions in the symmetrical or asymmetrical stator winding configurations.

The proposed control approach has been used to implement a three-phase direct flux vector control (DFVC) scheme [29] for the regulation of the stator flux and torque of a multi-three-phase induction machine (IM). A 12-phase IM prototype with a quadruple-three-phase stator winding configuration, rated 10 kW at 6000 r/min, has been used to validate the proposed method.

This paper expands [30] and brings in added value by including the following aspects:

1) An in-depth analysis of the proposed control approach to demonstrate how it can be used to define matrix transformations that deal with any multi-three-phase configuration, not only the symmetrical or asymmetrical ones, and still get similar results to the VSD approach.
2) More details about the proposed control scheme, including the description of control modules performing the flux-weakening (FW) operation with maximum torque per voltage (MTPV) limitation.
3) Additional experimental results to demonstrate the complete torque controllability of the machine in faulty conditions, including the performance under voltage and current constraints.

The paper is organized as follows. Machine modeling is described in Section II, while the proposed control scheme is shown in Section III. Experimental results are illustrated in Section IV. Finally, Section V provides paper conclusions.

II. MACHINE MODELING

The proposed control approach uses the DMS modeling to express the machine flux and torque. Therefore, in the following, the DMS approach is applied to a multi-three-phase squirrel-cage IM with p pole pairs and n winding sets. A sinusoidal distribution of the stator windings is assumed, i.e., they interact with each other and with the rotor only through the fundamental spatial component of the air-gap magnetic field. Mutual leakage fluxes and iron losses are not considered.

A. MS model of a multi-three-phase IM

The DMS approach is defined starting from the MS model of a generic multi-three-phase machine. According to [7], [27], the MS model of a multi-three-phase IM in stationary coordinates is obtained by applying the Clarke transformation to the equations of each winding set k ($k=1,...,n$) as [1]:

$$\bar{z}_{sk,\alpha\beta} = \left[T_{C,k} \right] \cdot \bar{z}_{sk,abc} \tag{1}$$

where $\bar{z}_{sk,abc}=[z_{sk,a}\ z_{sk,b}\ z_{sk,c}]^t$ and $\bar{z}_{sk,\alpha\beta}=[z_{sk,\alpha}\ z_{sk,\beta}]^t$ are generic k-set stator vectors in phase coordinates $(abc)_k$ and stationary coordinates $(\alpha\beta)$, respectively. Since each winding set has an isolated neutral point, the zero-sequence currents of the machine are zero, allowing to neglect them. Therefore, the amplitude-invariant Clarke transformation of each winding set k ($k=1,...,n$) is defined as follows:

$$\left[T_{C,k} \right] = \frac{2}{3} \cdot \begin{bmatrix} \cos\left(\vartheta_{sk}\right) & \cos\left(\vartheta_{sk}+2\pi/3\right) & \cos\left(\vartheta_{sk}+4\pi/3\right) \\ \sin\left(\vartheta_{sk}\right) & \sin\left(\vartheta_{sk}+2\pi/3\right) & \sin\left(\vartheta_{sk}+4\pi/3\right) \end{bmatrix} \tag{2}$$

where the angle ϑ_{sk} is defined as the position of the k-set first phase a_{sk} relative to the α-axis; the latter is assumed coincident with the first phase of the first set a_{s1}, as shown in Fig. 2.

The stationary equations are subsequently computed in rotating coordinates (xy) through the well-known rotational transformation [13]. In summary, the equation system of a generic winding set k ($k=1,...,n$) is computed as [7], [27]:

$$\begin{cases} \bar{v}_{sk,xy} = R_s \cdot \bar{i}_{sk,xy} + \dfrac{d}{dt}\bar{\lambda}_{sk,xy} + j \cdot \omega_{xy} \cdot \bar{\lambda}_{sk,xy} \\ \bar{\lambda}_{sk,xy} = k_r \cdot \bar{\lambda}_{r,xy} + L_{ls} \cdot \bar{i}_{sk,xy} + k_r \cdot L_{lr} \cdot \displaystyle\sum_{l=1}^{n} \bar{i}_{sl,xy} \\ \bar{0} = \dfrac{\bar{\lambda}_{r,xy}}{\tau_r} + \dfrac{d}{dt}\bar{\lambda}_{r,xy} + j \cdot \omega_{slip} \cdot \bar{\lambda}_{r,xy} - k_r \cdot R_r \cdot \displaystyle\sum_{l=1}^{n} \bar{i}_{sl,xy} \end{cases} \tag{3}$$

where $\bar{z}_{sk,xy}=[z_{sk,x}\ z_{sk,y}]^t$ and $\bar{z}_{sl,xy}=[z_{sk,x}\ z_{sk,y}]^t$ are generic stator vectors respectively defined for the winding sets k ($k=1,...,n$)
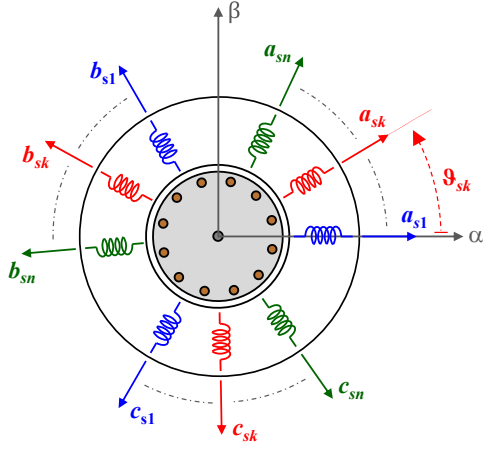
Fig. 2. Generic configuration of a multi-three-phase IM: angle displacement of the magnetic axes in one electrical revolution.

Fig. 3. Equivalent MS circuit of a multi-three-phase squirrel cage IM in stationary coordinates.

and l ($l=1,...,n$), both expressed in rotating coordinates (xy); $\bar{z}_{r,xy}=[z_{r,x}\ z_{r,y}]^t$ is a generic rotor vector expressed in rotating coordinates (xy); ω_{xy} and ω_{slip} are synchronous and slip speeds; v, i, and λ have the meaning of voltage, current, and flux linkage, respectively; R_s, L_{ls}, R_r, L_{lr}, k_r, and τ_r are the stator resistance, stator leakage inductance, rotor resistance, rotor leakage inductance, rotor coupling factor, and the rotor time-constant, respectively. Finally, j is the complex vector operator in matrix form, and $\bar{0}=[0\ 0]^t$.

By performing the machine power balance [7], the overall electromagnetic torque T is computed as:

$$T = \sum_{k=1}^{n} T_k = \frac{3}{2} \cdot p \cdot \sum_{k=1}^{n} \left(\bar{\lambda}_{sk,xy} \times \bar{i}_{sk,xy} \right) \qquad (4)$$

where T_k is the torque contribution of the kth winding set, while '$\times$' is the outer product operator. Based on (3), (4), it can be noted how the MS approach highlights the stator flux and the torque contribution of each winding set, resulting in suitable for the implementation of modular torque control schemes [7]. Further proof of the MS modularity is given in Fig. 3, showing the machine's equivalent circuit in stationary coordinates (L_m is the magnetizing inductance). Nevertheless, (3) shows that the winding sets are still magnetically coupled with each other, thus demonstrating that it is necessary to implement dedicated decoupling algorithms in the MS-based control schemes [7]. In this way, underdamped or even instability phenomena [24] are prevented.

B. DMS model of a multi-three-phase IM

According to [27], the DMS approach aims at removing the MS couplings between the winding sets, thus obtaining a machine model quite similar to that of the VSD approach but preserving the modularity. In detail, a decoupling transformation is applied to the MS model (3), leading to the definition of common- and differential-mode subspaces. According to [27], the decoupling method consists of the following decoupling transformation:

$$\begin{Bmatrix} \bar{z}_{scm,xy} \\ \bar{z}_{sdm-1,xy} \\ ... \\ \bar{z}_{sdm-(n-1),xy} \end{Bmatrix} = [T_D] \cdot \begin{Bmatrix} \bar{z}_{s1,xy} \\ \bar{z}_{s2,xy} \\ ... \\ \bar{z}_{sn,xy} \end{Bmatrix} \qquad (5)$$

It is noted how each MS stator variable (v,i,λ), defined for each winding set, in turn, is decomposed in terms of *one* common-mode vector $\bar{z}_{scm,xy}=[z_{scm,x}\ z_{scm,y}]^t$ and ($n-1$) differential-mode vectors $\bar{z}_{sdm-u,xy}=[z_{sdm-u,x}\ z_{sdm-u,y}]^t$ ($u=1,..,n-1$). Concerning the decoupling transformation $[T_D]$, it is defined as:
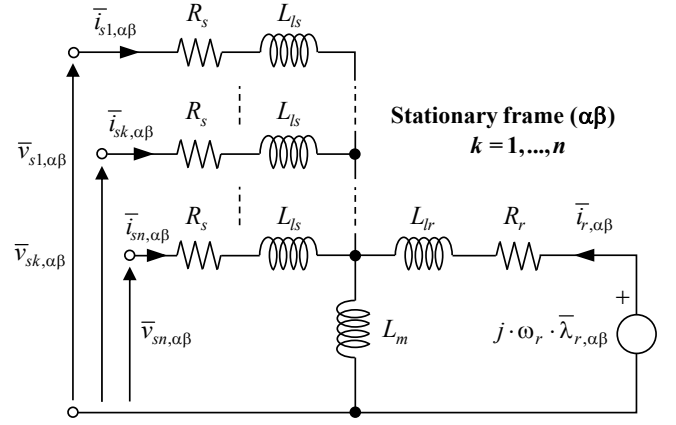
$$[T_D] = \frac{1}{n} \cdot \begin{bmatrix} I_2 & I_2 & I_2 & I_2 & ... & I_2 & I_2 & I_2 & I_2 \\ w_1 & q_1 & q_1 & q_1 & ... & q_1 & q_1 & q_1 & q_1 \\ 0_2 & w_2 & q_2 & q_2 & ... & q_2 & q_2 & q_2 & q_2 \\ 0_2 & 0_2 & w_3 & q_3 & ... & q_3 & q_3 & q_3 & q_3 \\ ... & ... & ... & ... & ... & ... & ... & ... \\ 0_2 & 0_2 & 0_2 & 0_2 & ... & 0_2 & w_{n-2} & q_{n-2} & q_{n-2} \\ 0_2 & 0_2 & 0_2 & 0_2 & ... & 0_2 & 0_2 & w_{n-1} & q_{n-1} \end{bmatrix} \quad (6)$$

where I_2 and 0_2 are the identity- and zero- 2×2 submatrices, respectively, while w_u and q_u ($u=1,...,n-1$) are 2×2 submatrices defined as follows:

$$w_u = \sqrt{\frac{n \cdot (n-u)}{(n-u+1)}} \cdot I_2 \quad , \quad q_u = -\sqrt{\frac{n}{(n-u) \cdot (n-u+1)}} \cdot I_2 \quad (7)$$

Therefore, the decoupling transformation is represented with a sparse matrix characterized by the amplitude invariant propriety with a power coefficient equal to n. For example, in a quadruple-three-phase machine ($n=4$), (6) is computed as:

$$[T_D]_{n=4} = \frac{1}{4} \cdot \begin{bmatrix} I_2 & I_2 & I_2 & I_2 \\ \sqrt{3} \cdot I_2 & -1/\sqrt{3} \cdot I_2 & -1/\sqrt{3} \cdot I_2 & -1/\sqrt{3} \cdot I_2 \\ 0_2 & 2\sqrt{2/3} \cdot I_2 & -\sqrt{2/3} \cdot I_2 & -\sqrt{2/3} \cdot I_2 \\ 0_2 & 0_2 & \sqrt{2} \cdot I_2 & -\sqrt{2} \cdot I_2 \end{bmatrix} \quad (8)$$

In summary, the DMS machine model is computed by merging (3) for all sets ($k=1,...,n$) and applying (5) and (6). Starting from the common-mode subspace, the following system of equations is thus obtained [27]:

$$\begin{cases} \bar{v}_{scm,xy} = R_s \cdot \bar{i}_{scm,xy} + \dfrac{d}{dt}\bar{\lambda}_{scm,xy} + j \cdot \omega_{xy} \cdot \bar{\lambda}_{scm,xy} \\ \bar{\lambda}_{scm,xy} = k_r \cdot \bar{\lambda}_{r,xy} + (L_{ls} + k_r \cdot n \cdot L_{lr}) \cdot \bar{i}_{scm,xy} \\ \bar{0} = \dfrac{\bar{\lambda}_{r,xy}}{\tau_r} + \dfrac{d}{dt}\bar{\lambda}_{r,xy} + j \cdot \omega_{slip} \cdot \bar{\lambda}_{r,xy} - k_r \cdot n \cdot R_r \cdot \bar{i}_{scm,xy} \end{cases} \quad (9)$$

while the system of equations for each differential-mode subspace u ($u = 1,..,n-1$) is computed as:

$$\begin{cases} \bar{v}_{sdm-u,xy} = R_s \cdot \bar{i}_{sdm-u,xy} + \dfrac{d}{dt}\bar{\lambda}_{sdm-u,xy} + j \cdot \omega_{xy} \cdot \bar{\lambda}_{sdm-u,xy} \\ \bar{\lambda}_{sdm-u,xy} = L_{ls} \cdot \bar{i}_{sdm-u,xy} \end{cases} \quad (10)$$

Finally, the overall electromagnetic torque is computed as:

$$T = 1.5 \cdot n \cdot p \cdot \left(\bar{\lambda}_{scm,xy} \times \bar{i}_{scm,xy} \right) \qquad (11)$$

It can be noted that the DMS machine model is similar to that obtained by using the VSD approach. Indeed, the electromagnetic and torque equations that rule the common-mode (9), (11) are formally identical to those obtained for
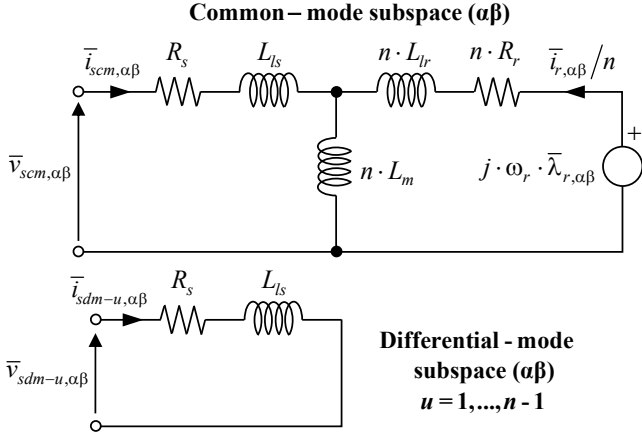
Common − mode subspace (αβ)

Fig. 4. Equivalent DMS circuit of a multi-three-phase squirrel cage IM in stationary coordinates.

Fig. 5. Asymmetrical quadruple-three-phase winding configuration with winding set 3 faulty (dashed green windings).

the main subspace through the VSD. More details about the VSD-based modeling are reported in [27], as well as in the literature concerning the multiphase machines [11], [12]. Further proof of the similarity between the VSD and DMS modeling approaches is given in Fig. 4, showing the DMS machine's equivalent circuit in stationary coordinates.

Furthermore, it is noted that the differential-mode subspaces do not participate in the electromechanical energy conversion. They represent the unbalance between the winding sets regarding currents, flux, or both. This propriety is also encountered in the VSD time-harmonic subspaces. However, the meaning of such subspaces is different from that of the DMS differential-mode ones. Based on how the VSD matrix transformation is computed [11], [14], the VSD time-harmonic subspaces represent specific time-harmonic patterns of the machine. Conversely, the DMS differential-mode subspaces are obtained as linear combinations of the fundamental-time models of the machine's winding sets. Further proof of this is given in [28], where it is shown how the DMS differential-mode subspaces do not possess the same properties as the VSD time-harmonic ones in terms of time-harmonic decoupling [14], [28], [31]. Therefore, DMS-based control schemes are impractical if time-harmonic injection or compensation strategies must be performed [8], [31].

In summary, the DMS approach allows removing the MS couplings among the machine's winding sets. Nevertheless, compared to VSD-based modeling, the modularity is preserved. Indeed, according to (5)-(7), the common- and differential- mode vectors are directly computed as numeric linear combinations of the MS variables belonging to the winding sets.

C. Proposed approach: adaptive DMS (A-DMS) modeling

Compared to the VSD modeling, the DMS approach presents the following features:

- The decoupling transformation $[T_D]$ is defined regardless of the stator winding configuration since it is applied directly to the MS machine model. Therefore, the limitations of the VSD when it comes to irregular winding configurations are analytically overcome without using numerical workarounds [32].
- No constraints exist on applying the decoupling transformation to a specific group of machine winding sets, thus modeling in terms of common- and differential- mode subspaces only the system of equations associated with such a group.

Such features become useful for control solutions that have to manage the operation of a multi-three-phase machine after an open-three-phase fault event.
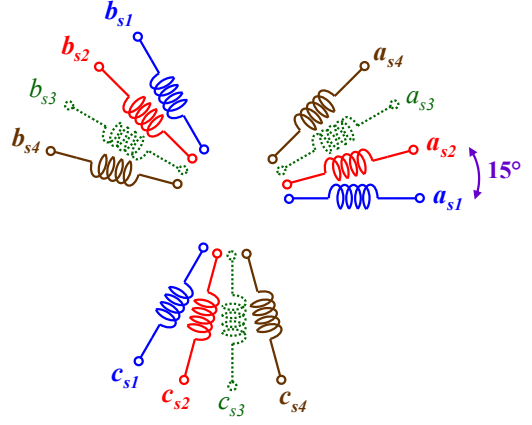
Indeed, in balanced operation among the units under machine healthy conditions, both the VSD- and DMS- based control solutions perform the torque regulation by actively managing only their principal subspace, i.e., the fundamental subspace for the VSD while the common-mode subspace for the DMS solution. This allows the implementation of the control system of a multi-three-phase machine through the same control structures of three-phase motor drives [13].

Nevertheless, if an open three-phase fault occurs, the VSD- and DMS- based control schemes need the active control of the secondary subspaces to keep the machine currents balanced and within their boundaries, as well as continuity of the torque production. In other words, the implementation of additional control modules with dedicated fault-tolerant strategies is necessary to manage the time-harmonic subspaces for the VSD-based solutions [6] and the differential-mode subspaces for the DMS ones [27]. As a result, the simplicity that characterizes the VSD-based and DMS-based control schemes is lost.

A solution to avoid the scenario mentioned above is to adapt the machine modeling by considering a stator winding configuration consisting of only healthy/active winding sets. According to the literature, such a solution is not viable for VSD-based modeling since the post-fault configuration of the stator winding hardly satisfies the constraint of being symmetrical or asymmetrical [14]. Consequently, the definition of a dedicated transformation for VSD is not possible without numerical methods [32].

Conversely, thanks to the properties previously mentioned, the DMS-based control schemes always allow changing on-the-fly the decoupling transformation, i.e., adapting it to the post-fault configuration of the stator winding. Thus, defining a so-called adaptive DMS (A-DMS) modeling is possible. In the following, a practical example is reported. Let us assume that the winding set 3 of an asymmetrical quadruple-three-phase machine becomes faulty. The post-fault configuration of the stator winding is shown in Fig. 5. According to the literature, a VSD transformation cannot be defined for this configuration because it is neither symmetrical nor asymmetrical. However, the DMS modeling allows adapting the decoupling transformation (6) by setting the number n to that of active winding sets, i.e., $n = 3$ as:

$$[T_D]_{n=3} = \frac{1}{3} \cdot \begin{bmatrix} I_2 & I_2 & I_2 \\ \sqrt{2} \cdot I_2 & -1/\sqrt{2} \cdot I_2 & -1/\sqrt{2} \cdot I_2 \\ 0_2 & \sqrt{3/2} \cdot I_2 & -\sqrt{3/2} \cdot I_2 \end{bmatrix} \quad (12)$$

The adapted decoupling transformation is thus applied only to the healthy/active winding sets (1, 2, and 4) as follows:
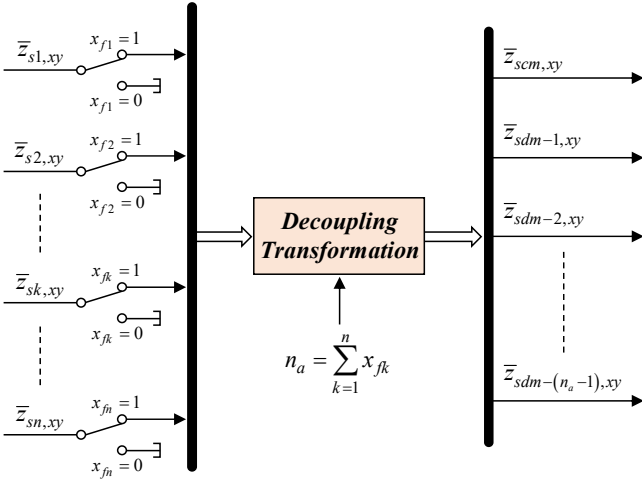
Fig. 6. Application scheme of the adaptive decoupling transformation.

$$\begin{Bmatrix} \overline{z}_{scm,xy} \\ \overline{z}_{sdm-1,xy} \\ \overline{z}_{sdm-2,xy} \end{Bmatrix} = \left[T_D \right]_{n=3} \cdot \begin{Bmatrix} \overline{z}_{s1,xy} \\ \overline{z}_{s2,xy} \\ \overline{z}_{s4,xy} \end{Bmatrix} \qquad (13)$$

Therefore, the resulting A-DMS model of the machine corresponds to (9)-(11) but considers three winding sets ($n = 3$) and two differential-mode subspaces instead of three.

As a rule, a differential-mode subspace is removed from each winding set that becomes faulty. In parallel, the definition of the common-mode subspace and the remaining differential-mode ones is adapted according to (6), where the number n_a of healthy/active sets has to be considered instead of the effective/rated number n. In practical terms, the A-DMS machine model is obtained by considering only the healthy/active sets in (5) and by setting $n = n_a$ in (6), (7), and (9)-(11). For better understanding, the scheme of the adaptive decoupling transformation for a generic variable z (v, i, λ) is shown in Fig. 6.

The variable x_{fk} stands for the status (0=faulty,1=healthy) of the generic winding set k ($k=1,...,n$). If the generic winding set k is faulty, the related MS variables are automatically excluded from the computation of the common- and differential-mode vectors. The advantages of the A-DMS approach are thus evident if a balanced operation among the healthy winding sets is assumed, regardless of the machine operating conditions (healthy or faulty). This scenario is typical in high-power applications (e.g., oil and gas [10]). For such cases, only the common-mode subspace is permanently active. Conversely, the differential-mode currents are always zero, regardless of the machine operating conditions (healthy or faulty) and the actual number of healthy winding sets.

In summary, an A-DMS-based electric drive can control the torque of a multi-three-phase machine both in healthy and faulty operation by controlling only the common-mode subspace and allowing the use of any control scheme developed for the three-phase drives without additional control modules or specific fault-tolerant control strategies. In this way, the simplicity of the control structure is preserved in any operating condition. The only constraint is that the healthy winding sets must be balanced with each other. However, this scenario usually happens in practice since the stator Joule losses of the machine are minimized [8].

D. A-DMS modeling: full-order matrix transformations

Another significant advantage of the A-DMS modeling is the possibility to define full-order matrix transformations that

can be directly applied to the machine model in phase coordinates $(abc)_k$ ($k=1,...,n$) to perform the following actions:

i) computation of the machine model in stationary coordinates;

ii) decoupling action to remove the magnetic coupling among the winding sets.

For clarity, the VSD matrix transformation is the most known example of a full-order matrix transformation performing the actions above. However, it can be computed only for symmetrical or asymmetrical stator winding configurations [14]. Conversely, the full-order matrix transformations obtained using the A-DMS modeling can be applied to any multi-three-phase configurations while still getting similar results to the VSD approach, as demonstrated previously in (9)-(11). For brevity, the computation method of full-order matrix transformations using the A-DMS approach is reported in Appendix.

III. CONTROL SCHEME

In this paper, the A-DMS approach is proposed to implement the three-phase direct flux vector control (DFVC) scheme [29] to regulate the stator flux and torque of a multi-three-phase IM.

According to [29], the three-phase DFVC scheme is implemented in rotating stator flux coordinates ($xy \equiv dqs$). Therefore, the ds-axis position ϑ_s corresponds with that of the stator flux vector, as shown in Fig. 7. Since the (dqs) frame is adopted, the synchronous speed ω_s is defined as the angular speed of the stator flux vector to the stationary α-axis. Finally, the machine load-angle δ is defined as the ds-axis position to the rotor flux vector, where the latter determines the conventional d-axis (see Fig. 7).

For a multi-three-phase IM, n stator flux vectors are defined (one for each winding set) [7]. Therefore, a three-phase DFVC scheme should be implemented to control each unit. This solution is mandatory if power-sharing strategies among the units are performed since significant unbalances between the winding sets in terms of flux, currents, or both are potentially introduced [7], [8]. In these operating conditions, the machine presents n different stator flux frames, making the modular control schemes like the MS-based DFVC the only viable solution [7].

Since both DMS and A-DMS modeling approaches can perform their decoupling action only if a single reference frame is adopted, the A-DMS-based DFVC scheme proposed in this paper can manage only a balanced operation among the healthy units. This means that the healthy units must operate with the same values of stator flux amplitude and torque.
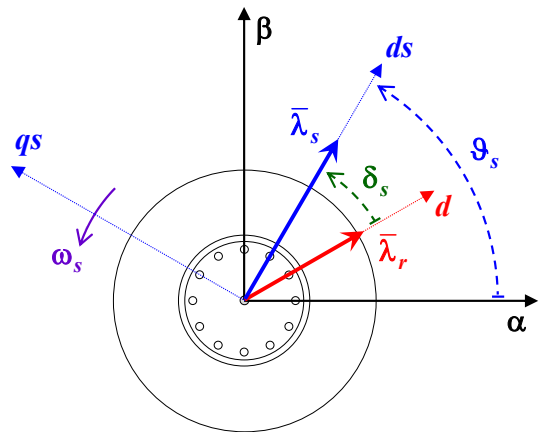

Fig. 7. Rotating stator flux frame (dqs) for a three-phase IM.

As demonstrated in [7], the stator flux vectors of the healthy units are overlapped in these operating conditions [27], allowing the definition of a unique active reference frame (dqs), i.e., an equivalent three-phase machine.

To help the understanding, the superscripts '~' and '^' are used in the following to denote an estimated- and observed-parameter/variable, respectively.

A. Flux and torque equations

Based on the A-DMS model, the flux and torque productions are performed in the common-mode subspace. Therefore, by considering (9) in the active frame (dqs), i.e., $\bar{\lambda}_{scm,dqs}=[\lambda_{scm}\ 0]^t$, the ds-axis voltage equation is computed as:

$$v_{scm,ds} = R_s \cdot i_{scm,ds} + \frac{d}{dt}\lambda_{scm} \qquad (14)$$

The flux amplitude of the healthy winding sets is regulated by the ds-axis common-mode voltage $v_{scm,ds}$. The machine torque can be directly regulated by the qs-axis common-mode current $i_{scm,qs}$, which has the meaning of the machine's torque-producing current. Proof of this statement is given by (11), expressed in the active frame (dqs), which leads to as follows:

$$T = 1.5 \cdot n_a \cdot p \cdot \lambda_{scm} \cdot i_{scm,qs} \qquad (15)$$

Finally, the qs-axis common-mode current $i_{scm,qs}$ is regulated by the qs-axis common-mode voltage $v_{scm,qs}$, as for the conventional three-phase DFVC scheme [29].

B. Stator flux observer

Like the DMS-based DFVC scheme, the proposed control solution needs to implement a flux observer to estimate the stator flux vectors of all winding sets. In this way, the common- and differential- mode values of stator fluxes amplitudes can be computed, as well as the active stator frame (dqs) used to calculate the torque-producing currents of the machine. The adopted stator flux observer is shown in Fig. 8, whose structure is the same implemented for the MS-based and DMS-based DFVC schemes [7], [27].

A reduced-order observer is implemented for each three-phase winding set k ($k = 1,...,n$). In this way, the estimate of the stator flux vector of each three-phase winding set is independent of the other ones, allowing a straightforward post-fault operation after losing one or more three-phase units. As shown in Fig. 8, the k-unit flux observer combines two model-based estimators implemented in the stationary coordinates ($\alpha\beta$). The first one is based on the k-set voltage model (VI) and obtains the estimate of the k-set stator flux vector by time-integrating the k-set back-electromotive force (back-emf) as follows:

$$\bar{\lambda}_{sk,\alpha\beta} = \int \left(\bar{v}_{sk,\alpha\beta} - R_s \cdot \bar{i}_{sk,\alpha\beta} \right) dt \qquad (16)$$

According to Fig. 8, it is noted that the k-set back-emf is integrated using the Euler discretization, where T_s is the sampling time of the digital controller. The VI-based estimator relies on reconstructing the k-set phase-voltages from the k-set duty-cycles and inverter dc-link voltage. Therefore, as known from the literature [33], the voltage estimation is affected by the voltage errors of the k-set inverter module at low speed. However, this estimator gets a high observation accuracy in the medium/high-speed range of the machine [7].

To get high observation accuracy in the low-speed range of the machine, each k-set flux observer relies on the stator flux estimate provided by the second estimator, whose operation is based on the k-set current model (Iϑ). The Iϑ-based estimator is immune to the voltage errors introduced by the k-set inverter module since it implements the currents-to-
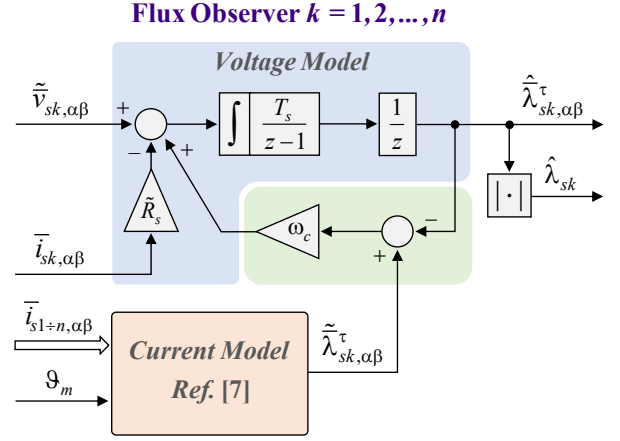

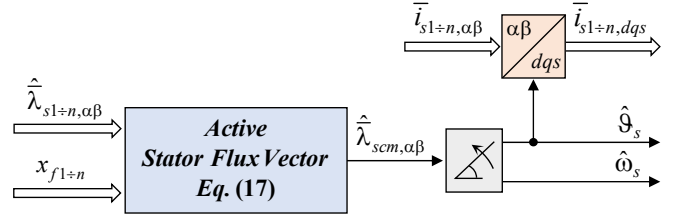Fig. 8. Stator flux observer of a generic winding set k ($k=1,...,n$).

Fig. 9. Computation of position and speed of the (dqs) frame and (dqs) components of the k-set phase-currents.

flux relationships of the machine. More details about the Iϑ-based estimator are reported in [7].

The crossover frequency (rad/s) between the Iϑ-based estimator and the VI-based one is established through the observer's gain ω_c (see Fig. 8) [7], whose value in the validation stage has been set at 125 rad/s (near 20 Hz) for all three-phase units.

According to Fig. 9, the estimates of the flux vectors of all winding sets are used to compute the active stator frame (dqs). Therefore, the average stator flux vector that represents the healthy units, i.e., corresponding to the common-mode stator flux vector using the A-DMS modeling $\bar{\lambda}_{scm,\alpha\beta}$, is calculated as a function of the units' states x_{fk} ($k=1,...,n$) as follows:

$$\hat{\bar{\lambda}}_{scm,\alpha\beta} = \frac{\sum_{k=1}^{n}\left(x_{fk} \cdot \hat{\bar{\lambda}}_{sk,\alpha\beta} \right)}{\sum_{k=1}^{n} x_{fk}} = \frac{1}{n_a} \cdot \sum_{k=1}^{n}\left(x_{fk} \cdot \hat{\bar{\lambda}}_{sk,\alpha\beta} \right) \qquad (17)$$

For the sake of simplicity, it is assumed that the units' states x_{fk} ($k=1,...,n$) are input signals of the proposed control scheme. Once the stationary components of the average stator flux vector are computed, the position ϑ_s and the synchronous speed ω_s of the active stator frame (dqs) are calculated (see Fig. 9). In this way, the (dqs) components of the phase-currents of each set k ($k = 1,...,n$) are obtained using the rotational transformation [13]. Finally, it is highlighted how the synchronous speed ω_s is calculated using a phase-locked loop (PLL) linked to the stationary components of the average stator flux vector. Thus, avoiding implementing the discrete-time derivative of the ds-axis position ϑ_s.

C. Adaptive decoupling transformation

The proposed drive scheme regulates the machine torque by directly controlling the common-mode values of flux amplitude and torque-producing current. In parallel, the flux amplitude and qs-axis current of each differential-mode subspace are controlled at zero.
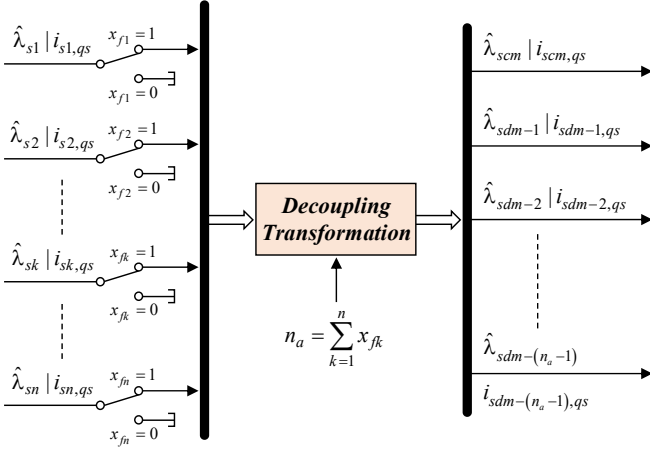
Fig. 10. Adaptive computation of the common- and differential modes of flux amplitudes and torque-producing currents.
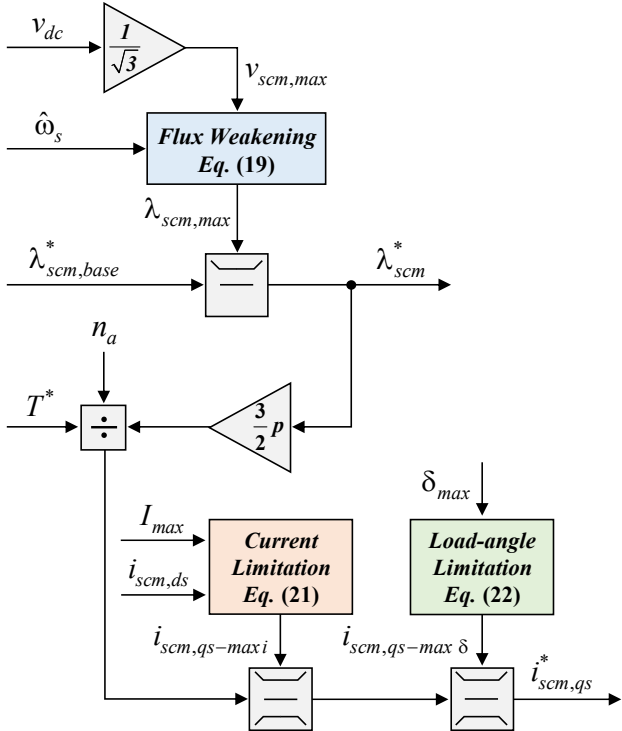

Fig. 11. A-DMS-based DFVC scheme: computation of the common-mode references of flux amplitude and torque-producing current.

Therefore, the adaptive decoupling transformation $[T_D]$ is applied to the flux amplitudes and torque-producing currents of the healthy winding sets, leading to the computation of the corresponding values of common- and differential- mode. The application of the adaptive decoupling transformation on the observed stator flux amplitudes and measured torque-producing currents is shown in Fig. 10.

D. Stator flux and torque-producing current references

The control solution proposed in this paper is similar to that reported in [27], where a DMS-based DFVC is presented. The main difference consists in how the machine's post-fault operation is performed. In [27], the decoupling transformation $[T_D]$ has been kept invariant regardless of the machine's operating condition (healthy or faulty). Thus, the common- and differential- mode vectors are expressed as a function of the variables belonging to both healthy and faulty winding sets. Therefore, to perform the machine's post-fault operation, the computation of the reference- and observed- value of the

flux amplitude belonging to each faulty winding set is necessary [27]. Also, such values must be computed in the reference frame of the active units (dqs). Finally, since both references of flux amplitude and torque-producing current belonging to the faulty winding sets differ from those of the healthy ones, the active control of the differential-mode subspaces is automatically performed after applying the decoupling transformation [27]. In this way, the phase-currents of the healthy sets are kept balanced and within their boundaries. In summary, it is evident that the DMS-based DFVC scheme requires implementing specific control modules to perform the machine's post-fault operation properly. More details are reported in [27].

Unlike the DMS-based DFVC scheme, the proposed solution is based on A-DMS modeling. Therefore, if an open-three-phase fault occurs, the definition of the common- and differential- mode subspaces is adapted to consider the stator winding's post-fault configuration. In this way, the common-mode references of flux amplitude λ_{scm}^* and torque-producing current $i_{scm,qs}^*$ are computed easily, as shown in Fig. 11.

If the machine is operated below the base speed, the common-mode flux reference (corresponding to that of each healthy winding set) is set to a predefined base value $\lambda_{scm,base}^*$ usually equal to the machine's rated flux:

$$\lambda_{scm,base}^* = \lambda_{s,rated} \tag{18}$$

The flux reference can be optimized by following the maximum torque per ampere profile (MTPA) of the machine [34], which maximizes the overload capability of the drive both in healthy and faulty operation since the overall Joule losses are minimized.

According to Fig. 11, the common-mode flux reference is limited above the base speed to ensure the flux-weakening operation (FW). The FW operation is performed similarly to the three-phase DFVC scheme [29], using a model-based law that avoids the implementation of an outer voltage controller (as for FOC schemes [35]). Therefore, by manipulating the common-mode voltage equation (9) computed in rotating (dqs) coordinates, the following FW law is implemented:

$$\lambda_{scm}^* \leq \lambda_{scm,max} \simeq \frac{v_{scm,max} - \tilde{R}_s \cdot i_{scm,qs} \cdot sign(\hat{\omega}_s)}{|\hat{\omega}_s|} \tag{19}$$

where the common-mode voltage limit $v_{scm,max}$ corresponds to the voltage constraint imposed by the inverter feeding the machine, i.e., $v_{dc}/\sqrt{3}$, where v_{dc} is the dc-link voltage. The implementation of (19) is simple, as it requires the knowledge of the stator resistance R_s and synchronous speed of the (dqs) frame ω_s.

Since a balanced operation among the units is considered, the torque contributions of the healthy winding sets are identical to each other. Hence, the reference of the common-mode torque-producing current $i_{scm,qs}^*$ of each healthy winding set is computed according to (15) as:

$$i_{scm,qs}^* = T^* / \left(1.5 \cdot n_a \cdot p \cdot \lambda_{scm}^*\right) \tag{20}$$

where T^* is the machine torque reference. However, according to the three-phase DFVC scheme [29], the reference of the common-mode torque-producing current is limited to satisfy the following constraints:

i) keeping the machine's phase currents within their boundary I_{max};
ii) performing the MTPV operation in deep FW operation, i.e., avoiding the machine's load angle δ overcomes its maximum limit δ_{max}.

Therefore, according to the constraints above, the reference of the common-mode torque-producing current is first limited regardless of its sign as follows:

$$\left| i_{scm,qs}^* \right| \le i_{scm,qs-max\,i} = \sqrt{I_{max}^2 - i_{scm,ds}^2} \qquad (21)$$

Instead, the MTPV operation is performed using the same procedure reported in [27] and hereafter briefly summarized:

$$\left| i_{scm,qs}^* \right| \le i_{scm,qs-max\,\delta} = \frac{\tilde{k}_r \cdot \hat{\lambda}_r}{\tilde{L}_{ls} + n_a \cdot \tilde{k}_r \cdot \tilde{L}_{lr}} \cdot \sin(\delta_{max}) \quad (22)$$

However, it is highlighted that the application of (22) in this paper is different from that reported in [27]. Indeed, in [27], (22) is used to limit the torque-producing current reference of each active unit. After, the decoupling transformation $[T_D]$ computed considering all machine's winding sets ($n_a = n$) is applied to the references of torque-producing currents of all units (healthy and faulty), thus computing their corresponding common- and differential mode values. Conversely, in this paper, (22) is used to limit the reference of common-mode torque-producing current directly, greatly simplifying the control scheme. According to [7], [13], [29], the load angle limit δ_{max} that performs the MTPV operation is 45 electrical degrees, avoiding the machine pull-out.

Finally, according to the A-DMS approach, the references of flux amplitude and qs-axis current of each differential-mode subspace u ($u = 1,...,n_a-1$) are permanently set to zero regardless of the machine operating conditions (healthy or faulty):

$$\lambda_{sdm-u}^* = 0 \quad , \quad i_{sdm-u,qs}^* = 0 \qquad \forall u = 1,...,n_a - 1 \quad (23)$$

E. Conventional DMS-based DFVC scheme

To better appreciate the simplicity of the A-DMS-based DFVC scheme, a representation of the conventional DMS-based scheme is shown in Fig. 12. It is noted that, for each unit k ($k = 1,...,n$), a dedicated three-phase DFVC scheme is implemented to compute the k-set references of flux amplitude λ_{sk}^* and torque-producing current $i_{sk,qs}^*$.

Conversely, in the A-DMS-based DFVC scheme, the three-phase DFVC scheme reported in Fig. 11 is executed only once to compute the common-mode references of flux amplitude λ_{scm}^* and torque-producing current $i_{scm,qs}^*$. Also, in the DMS-based DFVC scheme, the reference of flux amplitude for the faulty units must be computed using dedicated fault-tolerant control modules, as shown in Fig. 12. More details are reported in [27] since they are beyond the aim of this paper.
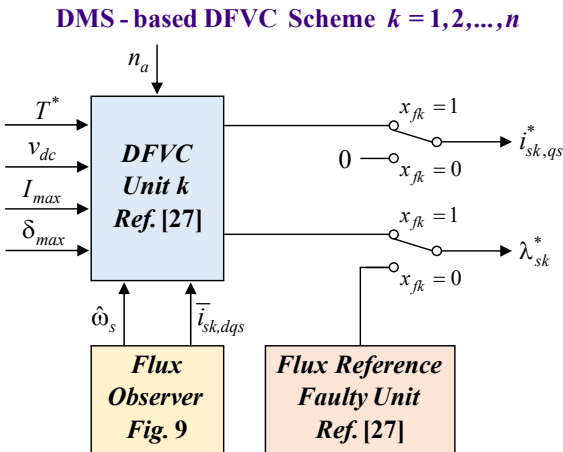
The decoupling transformation $[T_D]$, computed by considering the effective machine winding sets n, is finally applied to the winding sets' references of flux amplitude and torque-producing current, leading to the computation of the corresponding values of common- and differential- mode (see Fig. 13).

F. Flux and torque control

The flux and torque control of the machine is performed by actively controlling the common-mode values of flux amplitude and torque-producing current. In this paper, the use of conventional proportional-integral (PI) controllers is proposed (see Fig. 14) since the common-mode variables are dc quantities in steady-state conditions [27]. The number of PI regulators performing the control of the differential-mode subspaces depends on the machine's operating conditions. According to the A-DMS modeling, the number of existing differential-mode subspaces is equal to that of healthy winding sets n_a minus one. Therefore, in the extreme case of one healthy winding set, the machine control is performed only through the common-mode regulators since the differential-mode subspaces do not exist anymore. In other words, the operation of the multi-three-phase machine collapses into its simplest case, an actual three-phase motor, which requires only two PI regulators to perform the torque control.

Conversely, the number of differential-mode subspaces, with related PI regulators, in the DMS-based schemes does not change as the decoupling transformation is kept invariant regardless of the machine's operating conditions (healthy or faulty). Moreover, the differential-mode subspaces must be actively controlled in faulty conditions, while the differential-mode quantities must always be null in the A-DMS-based DFVC scheme. Regarding the latter, in the cases of IMs characterized by a negligible spatial-harmonic content in the air gap, it may even be possible to set the differential-mode voltage references at zero directly. In this way, no differential-mode controllers are needed, further simplifying the structure of the A-DMS-based schemes.

Considering the A-DMS-based solution in which both the common- and differential- mode quantities are controlled using PI regulators, the outputs of these last correspond to the reference voltages of the machine in terms of common- $\bar{v}_{scm,dqs}^*$ and differential- mode $\bar{v}_{sdm-u,dqs}^*$ ($u = 1,...,n_a-1$) (see Fig. 14).

DMS - based DFVC Scheme

Fig. 12. Computation of the k-set references ($k = 1,...,n$) of flux amplitude and torque producing current in the DMS-based DFVC scheme.
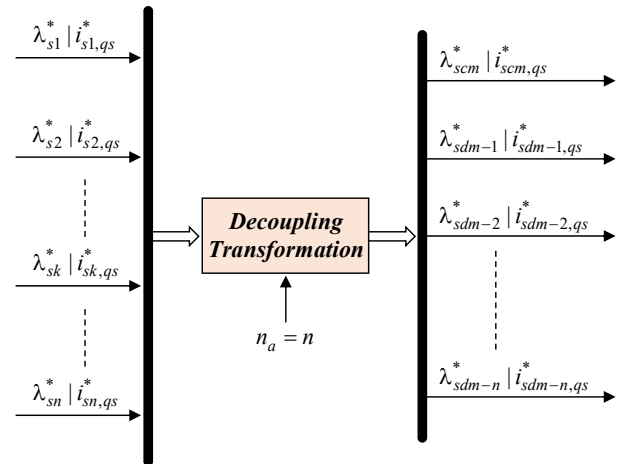

Fig. 13. Computation of common- and differential- mode references of flux amplitudes and torque-producing currents in the DMS-based DFVC scheme.
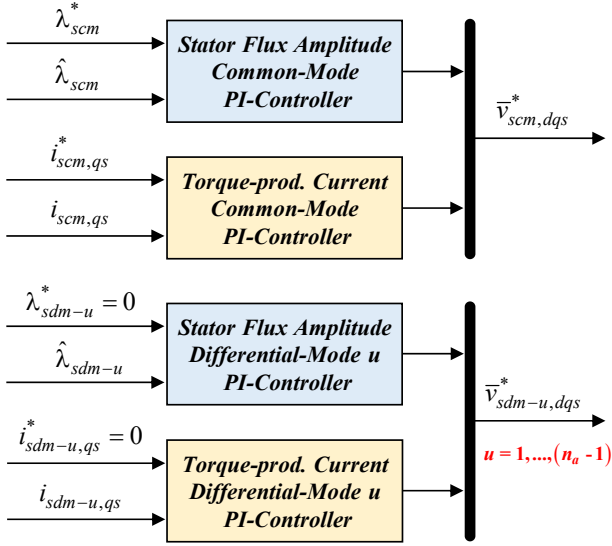
Fig. 14. Adaptive regulation of the common- and differential- modes of fluxes amplitudes and torque-producing currents using PI controllers.
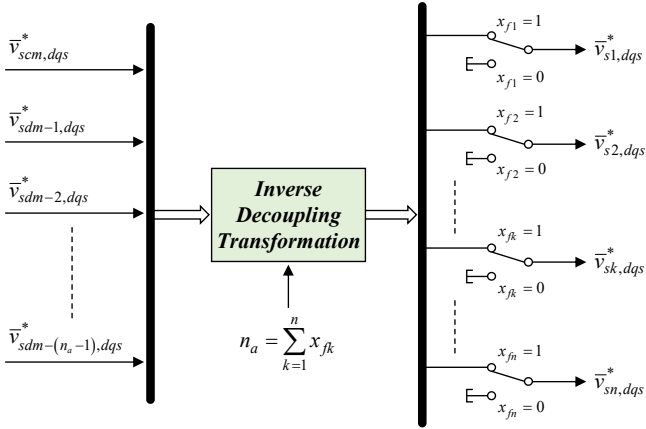

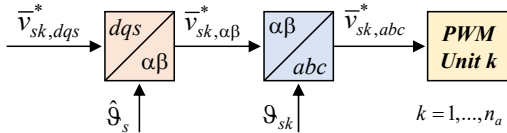Fig. 15. Computation of the reference voltages of the units by using the inverse adaptive decoupling transformation.

Fig. 16. PWM modulation of each healthy unit k ($k=1,...,n_a$).

Therefore, the inverse decoupling transformation $[T_D]^{-1}$ is applied to get the reference voltages of the healthy units in the active (dqs) frame $\bar{v}^*_{sk,dqs}$ ($k=1,...,n_a$), as shown in Fig. 15. Finally, after applying the inverse rotational transformation [13] and the inverse Clarke transformations (2), the reference voltages of each active unit in phase-coordinates $\bar{v}^*_{sk,abc}$ ($k=1,...,n_a$) are computed, as shown in Fig. 16.

G. Pulsewidth modulation (PWM)

According to the multi-three-phase drive topology, each winding set is fed by a dedicated three-phase inverter module (see Fig. 1). The PWM modulators are independent of one another (see Fig. 16), allowing the implementation of the well-known three-phase modulation techniques [36], including the selective harmonic elimination strategies for high-power converters using thyristors or adopting multilevel structures [37]. In this paper, the duty-cycles of the inverter modules $\bar{d}^*_{k,abc}$ ($k=1,...,n_a$) use the carrier-based space vector PWM (SV-PWM) in the experimental validation [36].
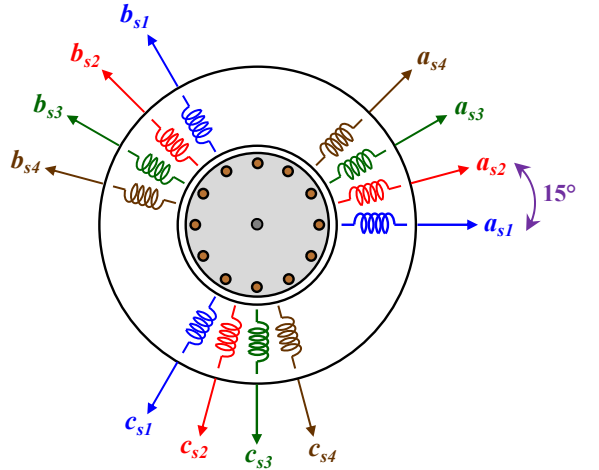
Fig. 17. Asymmetrical 12-phase IM using a quadruple-three-phase stator winding configuration.

TABLE I.   MACHINE PRIMARY DATA

Electrical Data	
Phase Number	12 (4·3-phase)
Pole number	4
Rated power	10 kW
Rated speed	6000 r/min
Rated phase-voltage	115 Vrms
Rated phase current	10 Arms
Machine Parameters	
Stator resistance R_s	145 mΩ
Stator leakage inductance L_{ls}	940 µH
Magnetizing inductance L_m	4.3 mH
Rotor resistance R_r	45 mΩ
Rotor leakage inductance L_{lr}	235 µH
Rated stator flux amplitude $\lambda_{s,rated}$	115 mVs
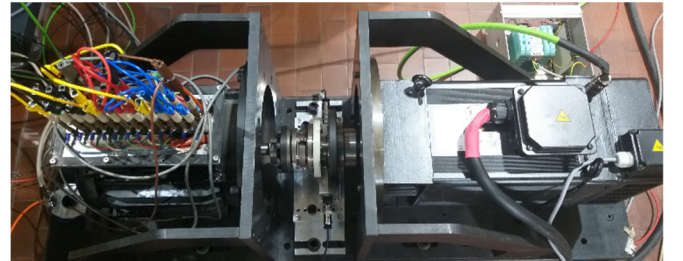
Fig. 18. View of the IM under test (left) and the driving machine (right).

IV. EXPERIMENTAL VALIDATION

The validation of the proposed control solution has been carried out on a 12-phase asymmetrical IM with four three-phase winding sets shifted by 15 electrical degrees (full-pitch windings with one slot/pole/phase), rated 10 kW at 6000 r/min (four poles) [38]. A schematic view of the stator winding's configuration is shown in Fig. 17, while Table I reports the primary machine data.

A. Test rig

The IM under test has been mounted on a test rig for validation purposes. The rotor shaft has been coupled to a driving machine acting as a prime mover, as shown in Fig. 18.

The power converter consists of four independent three-phase inverter power modules, rated 100 A/1200 V, fed at 270 V by a bidirectional dc source [39]. Both the switching- and sampling- frequencies have been set at 5 kHz to provide a compatible scenario with the industrial implementations [40].

Fig. 19. Drive configuration of a generic three-phase unit k ($k = 1,..,n$).

Finally, the digital controller is the dSPACE® DS1103 fast prototyping board, while the control algorithm has been developed in C-code.

The drive configuration of a generic unit k ($k = 1,...,n$) is shown in Fig. 19 and corresponds to the one used in a conventional three-phase drive. Therefore, the k-set phase-currents $\bar{i}_{sk,abc}$ and dc-link voltage v_{dc} are measured. Together with the feedback related to the three-phase units, the measurement of the rotor mechanical position ϑ_m is also taken, allowing the computation of the mechanical speed ω_m using a PLL. For the experimental validation, the rotor mechanical position has been measured using an incremental encoder with a resolution of 1024 pulses/r.

B. Experimental results

The experimental validation of the proposed control solution has been performed by replicating the same tests reported in [27]. In this way, a fair comparison between DMS- and A-DMS-based control approaches is possible. Both strategies achieve similar performance but implement two different fault-tolerant strategies. Indeed, a DMS-based control solution performs the post-fault drive operation by actively controlling the differential-mode subspaces, keeping the decoupling transformation $[T_D]$ invariant. In contrast, an A-DMS-based control solution performs the post-fault drive operation by changing on-the-fly the decoupling transformation $[T_D]$, thus redefining both common- and differential- mode subspaces according to the post-fault machine configuration. In this way, the differential- mode currents can be still kept null, actively controlling only the common-mode subspace using any of the conventional torque controllers for three-phase drives.

In summary, the A-DMS-based control solutions can be considered an evolution of the DMS-based ones since the control of the differential-mode subspaces is significantly simplified. According to [27], the experimental results are therefore provided for the drive operation with torque control mode and speed control mode. The latter has been implemented using an outer speed PI regulator, which provides the IM's reference torque T^* while the driving machine acts as an inertial load. Due to the mechanical limitation of the driving machine, the machine speed has been limited to 6000 r/min. Therefore, to test the drive operation in deep FW with MTPV within this speed range, the dc-link voltage has been halved at 135 V while performing the test in speed control mode.

Fig. 20. Inverter 3 shut-off in generation mode (-6000 r/min, 16 Nm). Ch1: $i_{s1,a}$ (10 A/div), Ch2: $i_{s2,a}$ (10 A/div), Ch3: $i_{s3,a}$ (10 A/div), Ch4: $i_{s4,a}$ (10 A/div). Time resolution: 5 ms/div.

Fig. 21. Inverter 3 shut-off in generation mode (-6000 r/min, 16 Nm). Time profiles of the MS variables in terms of torque (Nm), flux amplitudes (mVs), and torque-producing currents (A).

The amplitude limit of the phase-currents has been set at $I_{max} = 24$ A, allowing to test the overload operation of the three-phase units (rated current of 10 Arms, i.e., about 14.2 A peak). Also, with the possibility of overloading the units, it is possible to temporarily operate the machine at the rated torque even after the open-three-phase fault reported by one unit.

The regulators performing the flux- and current- controls (both common- and differential- mode) have been designed to get a small-signal bandwidth of the corresponding control loops of about 250 Hz. Finally, the PI regulator performing the speed control has been designed to get a small-signal bandwidth of the corresponding control loop of about 10 Hz (the mechanical inertia of the motor and prime mover is about 0.225 kg·m^2).

1) Experimental results in torque control mode

Starting from rated generating conditions (-6000 r/min, 16 Nm), the inverter power module 3 has suddenly been turned off, emulating a fault event reported by an inverter power module. The experimental results are shown in Figs. 20 – 23.

Fig. 20 shows the first phase-current '$i_{sk,a}$' (k=1,...,4) of each of the four three-phase sets before and after the fault. It is noted that the currents of the healthy units must increase to preserve the torque and machine flux. However, according to Figs. 22 – 23, only the common-mode subspace is actively controlled before and after the fault event.
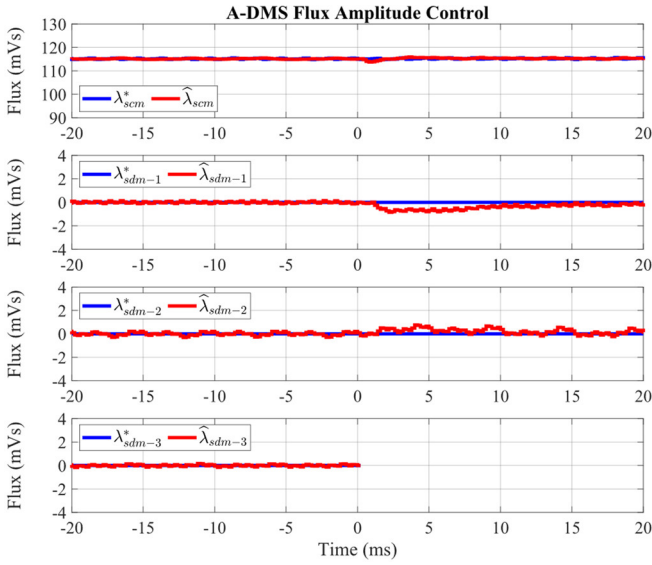
Fig. 22. Inverter 3 shut-off in generation mode (-6000 r/min, 16 Nm). Common- and differential- mode control of the fluxes amplitudes (mVs).
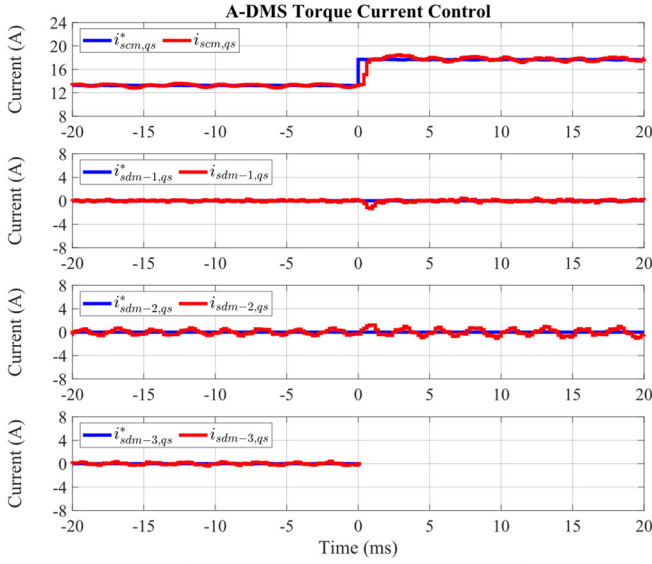

Fig. 23. Inverter 3 shut-off in generation mode (-6000 r/min, 16 Nm). Common- and differential- mode control of torque-producing currents (A).

According to (6), it is pointed out that the physical meaning of each common-mode variable consists of the average value of the respective components belonging to the healthy winding sets. Therefore, referring to Figs. 21 – 22, it is noted that the flux amplitude of the healthy sets (1,2,4) is kept at the rated value (115 mVs), while the common-mode torque-producing current increases from 13.2 to 17.7 A to satisfy the torque request (see Fig. 23). Due to machine asymmetries related to winding set 2 (see Fig. 21), it is noted that slight disturbances characterize the torque-producing current component belonging to the second differential-mode subspace (see Fig. 23). However, the phase currents of the healthy units are not affected by these machine asymmetries since they exhibit a sinusoidal waveform (see Fig. 20).

In summary, thanks to the A-DMS control approach, an open-three-phase fault event only leads to a change in the reference of the common-mode torque-producing current. The adaptive decoupling transformation automatically performs such a change without implementing any control strategies or additional control modules involving the differential-mode subspaces. Regarding the number of differential-mode subspaces, since all IM's units are active before the fault event, three differential-mode subspaces are controlled.
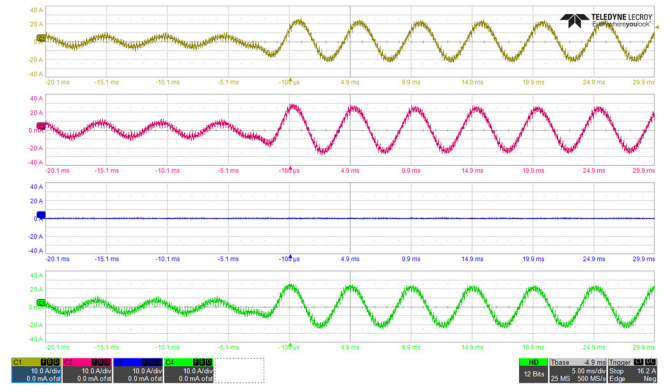

Fig. 24. Fast torque transient from no-load up to the rated generating conditions (-6000 r/min, 16 Nm) with unit 3 turned OFF. Ch1: $i_{s1,a}$ (10 A/div), Ch2: $i_{s2,a}$ (10 A/div), Ch3: $i_{s3,a}$ (10 A/div), Ch4: $i_{s4,a}$ (10 A/div). Time resolution: 5 ms/div.
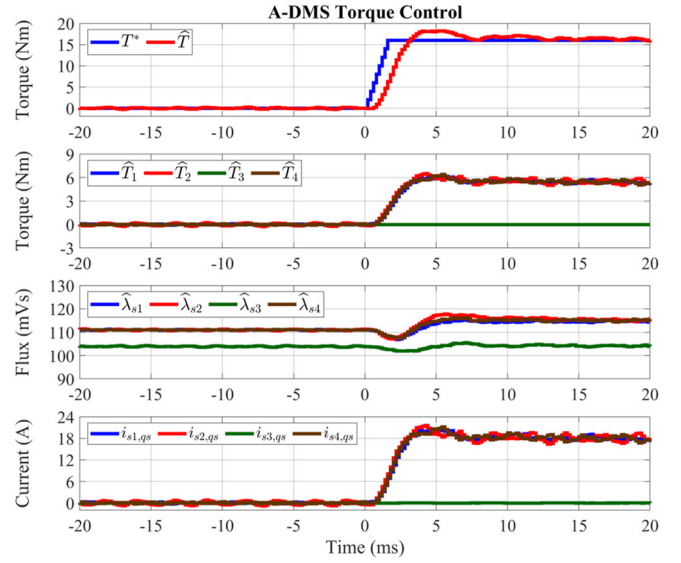

Fig. 25. Fast torque transient from no-load up to the rated generating conditions (-6000 r/min, 16 Nm) with unit 3 turned OFF. Time profiles of the MS variables in terms of torque (Nm), flux amplitudes (mVs), and torque-producing currents (A).
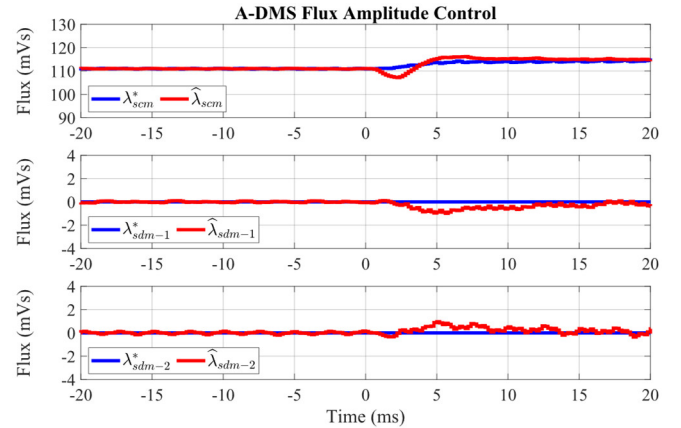

Fig. 26. Fast torque transient from no-load up to the rated generating conditions (-6000 r/min, 16 Nm) with unit 3 turned OFF. Common- and differential- mode control of the fluxes amplitudes (mVs).

However, according to the A-DMS approach, one unit is lost after the fault event, and the decoupling transformation for the post-fault stator winding configuration is redefined so that only two differential-mode currents are kept at zero. Therefore, the third differential-mode subspace, which does not exist anymore, is ignored after the fault event, as shown in Figs. 22 – 23, where the variables of the third differential-mode subspace are not plotted anymore.
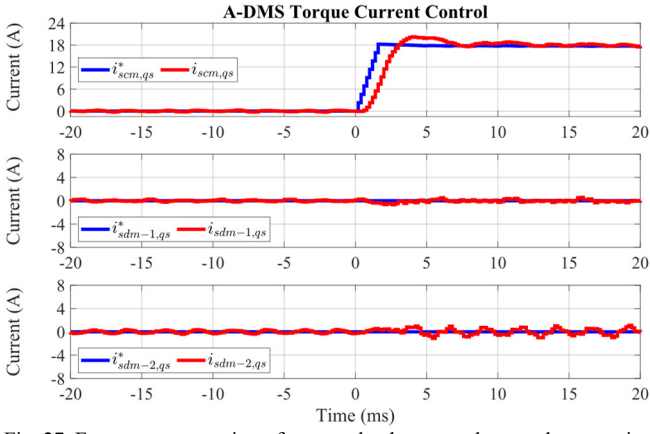
Fig. 27. Fast torque transient from no-load up to the rated generating conditions (-6000 r/min, 16 Nm) with unit 3 turned OFF. Common- and differential- mode control of torque-producing currents (A).

To demonstrate the dynamic performance of the torque control in faulty conditions, a fast torque transient (10 Nm/ms) from no-load up to the rated generating conditions (16 Nm, −6000 r/min), with unit 3 turned OFF, has been performed. The experimental results are shown in Figs. 24 – 27, demonstrating the full torque controllability when fast torque transients are performed since no significant overshoot (less than 15 %) on the currents/torque waveforms is reported.

According to Fig. 24, the phase-currents of the healthy units are perfectly sinusoidal both in no-load and rated torque conditions. Like the previous test, only the common-mode quantities of flux and torque-producing current have been actively controlled. Conversely, differential-mode currents and fluxes have been kept equal to zero according to the A-DMS control approach, as shown in Figs. 26 – 27.

Since the voltage limit was reached, the IM operated in FW in no-load conditions (common-mode flux amplitude at 110 mVs). However, in the rated generating conditions, iron losses, resistive voltage drops, and machine slip allowed to restore the machine stator flux to the rated value of 115 mVs, as shown in Fig. 26. Finally, slight disturbances due to the machine asymmetries affect the differential-mode subspaces when performing the fast torque transient. However, it can be noted how the PI controllers controlling the differential-mode fluxes and currents keep these quantities null without issues (see Figs. 26 – 27).

It is highlighted that the performance in torque control mode is the same reported in [27]. However, these results have been obtained by actively controlling only the common-mode subspace thanks to the A-DMS-based decoupling transformation. Conversely, the decoupling transformation has been kept invariant in [27], making it necessary to control the differential-mode subspaces actively.

2) Experimental results in speed control mode

The speed control mode has been tested by turning OFF units 1 and 3 to emulate another potential faulty condition of the drive. A step speed reference from 0 to 6000 r/min has been applied, and the corresponding results are shown in Figs. 28 – 31. Below the base speed, it is noted that the torque limit of each set (near 6 Nm) depends only on the current limit of the corresponding inverter units (I_{max} = 24 A). The FW operation starts near 2500 r/min, i.e., when the voltage limit of the inverter units is reached. According to Fig. 28, it is noted how the quasi-constant power range of the machine [41] starts from that speed value (P_m stands for the estimated mechanical power). In parallel, Fig. 29 shows how both flux amplitudes and torque-producing currents of the healthy sets
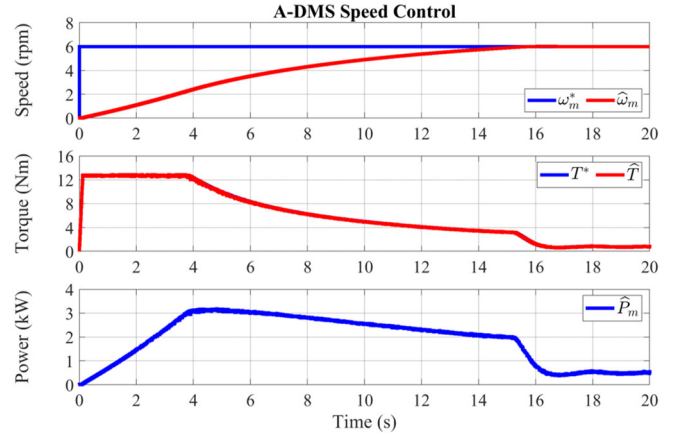

Fig. 28. Speed control from 0 to 6000 r/min with units 1 and 3 turned OFF. Time profiles of speed (r/min), torque (Nm), and mechanical power (kW).
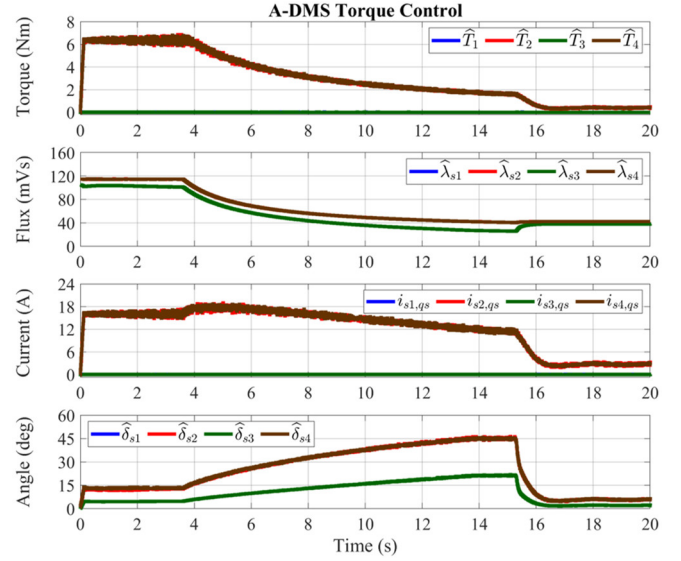

Fig. 29. Speed control from 0 to 6000 r/min with units 1 and 3 turned OFF. Time profiles of the MS variables in terms of torque (Nm), flux amplitudes (mVs), torque-producing currents (A), and load angles (deg).
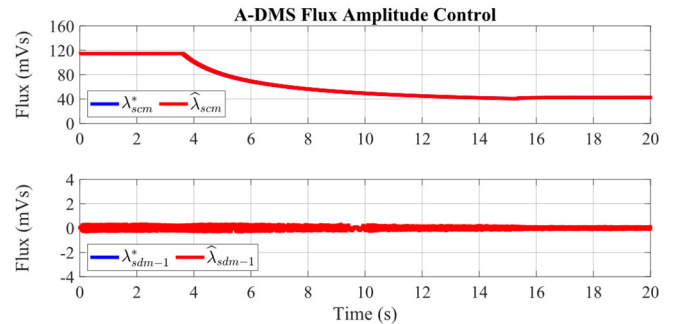

Fig. 30. Speed control from 0 to 6000 r/min with units 1 and 3 turned OFF. Common- and differential- mode control of the fluxes amplitudes (mVs).
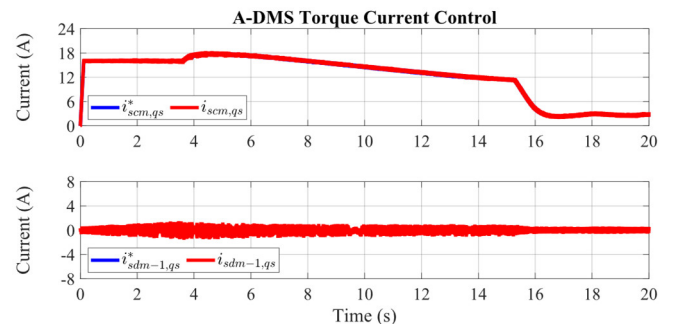

Fig. 31. Speed control from 0 to 6000 r/min with units 1 and 3 turned OFF. Common- and differential- mode control of torque-producing currents (A).

are properly controlled up to the maximum speed of 6000 r/min, corresponding to a significant FW ratio of about 1 : 3. Finally, the MTPV operation starts at about 5500 r/min, as confirmed by Fig. 29, which shows that the healthy units' load angles, i.e., δ_{s2} and δ_{s4}, are kept at their limit of 45 electrical degrees (δ_{max}) to avoid the machine pull-out.

According to Figs. 30 – 31, the torque control of the machine along the maximum torque per speed profile has been performed by actively controlling only the common-mode subspace. In addition, since only two winding sets were active, the decoupling transformation was redefined again with respect to the one used for the tests in torque control mode. Indeed, according to the A-DMS approach, only one differential-mode subspace has been managed since the second one has ceased to exist. Conversely, in [27], the same test performed by implementing a DMS-based DFVC scheme obtained the same results but by actively controlling both the common-mode subspace and all three differential-mode machine subspaces. Indeed, according to the DMS modeling, the decoupling transformation has been kept invariant regardless of the machine operating conditions.

V. Conclusion

The paper proposes an innovative control approach to perform the torque regulation of a multi-three-phase induction machine (IM) both in healthy and faulty operation (fault of one or more three-phase inverter modules) using any of the control schemes normally employed for three-phase drives.

The proposed control approach is based on the adaptive definition of the common- and differential- mode subspaces of the machine. In this way, the torque control of the latter can be performed by actively controlling only the common-mode subspace, keeping the differential-mode quantities of currents and fluxes always equal to zero regardless of the machine operating conditions (healthy or faulty).

The application of the proposed control approach allowed the use of the three-phase direct-flux vector control (DFVC) scheme to regulate both the stator flux and torque of a multi-three-phase IM having an arbitrary number of three-phase winding sets in any operating conditions and regardless of the configuration of the stator winding. However, it is highlighted how other control solutions like the conventional FOC-based current vector control can also be used.

The experimental validation has been carried out on a 12-phase IM that uses a quadruple-three-phase stator winding configuration. Experimental results validate the proposed control solution both in healthy and faulty machine operation. Also, the very good torque controllability of the machine in flux-weakening operation with maximum torque per volt limitation (MTPV) has been reported.

In conclusion, the advantages of the proposed control approach can be summarized as follows:
1) Any three-phase control scheme can be used to regulate the flux and torque of a multi-three-phase machine both in healthy and faulty operation without implementing specific control modules or strategies to perform the machine post-fault operation.
2) The stator winding configuration can be different from the symmetrical or asymmetrical ones since all the advantages of the decoupled multi-stator (DMS) modeling are preserved with the added value of keeping the control structure as simple as possible.

Appendix: A-DMS-Based Full-Order Matrix Transformations

Let us consider only the healthy/active sets of a generic multi-three-phase machine, sorted from 1 to n_a without loss of generality. Based on (2), a specific Clarke transformation is associated with the kth set ($k=1,...,n_a$). Therefore, the Clarke transformations of all healthy/active sets can be merged in a single matrix transformation $[T_C]$, which can be directly applied to the machine model in phase coordinates as follows:

$$\begin{Bmatrix} \overline{z}_{s1,\alpha\beta} \\ \overline{z}_{s2,\alpha\beta} \\ ... \\ \overline{z}_{sn_a,xy} \end{Bmatrix} = [T_C] \cdot \begin{Bmatrix} \overline{z}_{s1,abc} \\ \overline{z}_{s2,abc} \\ ... \\ \overline{z}_{sn_a,abc} \end{Bmatrix} \quad (24)$$

where:

$$[T_C] = \begin{bmatrix} [T_{C,1}] & 0_{2\times3} & ... & 0_{2\times3} \\ 0_{2\times3} & [T_{C,2}] & ... & 0_{2\times3} \\ ... & ... & ... & ... \\ 0_{2\times3} & 0_{2\times3} & ... & [T_{C,n_a}] \end{bmatrix} \quad (25)$$

In (25), $0_{2\times3}$ stands for a 2×3 submatrix containing only null elements.

Once (25) has been obtained, it can be combined with the decoupling transformation $[T_D]$ computed according to the A-DMS modeling approach, under the assumption to consider only the healthy winding sets of the machine, i.e., (6) calculated by setting $n = n_a$. Therefore, the A-DMS-based full-order matrix transformation $[T_F]$ performing a similar action to the VSD one but valid for all multi-three-phase configurations is computed, leading to the following result:

$$\begin{Bmatrix} \overline{z}_{scm,\alpha\beta} \\ \overline{z}_{sdm-1,\alpha\beta} \\ \overline{z}_{sdm-2,\alpha\beta} \\ ... \\ \overline{z}_{sdm-(n_a-1),\alpha\beta} \end{Bmatrix} = [T_D] \cdot [T_C] \cdot \begin{Bmatrix} \overline{z}_{s1,abc} \\ \overline{z}_{s2,abc} \\ \overline{z}_{s3,abc} \\ ... \\ \overline{z}_{sn_a,abc} \end{Bmatrix} = [T_F] \cdot \begin{Bmatrix} \overline{z}_{s1,abc} \\ \overline{z}_{s2,abc} \\ \overline{z}_{s3,abc} \\ ... \\ \overline{z}_{sn_a,abc} \end{Bmatrix} \quad (26)$$

The general form of $[T_F]$ is reported in (27). In addition, its computation for the most common multi-three-phase configurations in the literature [3], [5], [8], [12], [14], [31] is reported in the following figures:

- Penta-three-phase (15-phase as 5·3-phase): Fig. 32.
- Quad-three-phase (12-phase as 4·3-phase): Fig. 33.
- Triple-three-phase (9-phase as 3·3-phase): Fig. 34.
- Dual-three-phase (6-phase as 2·3-phase): Fig. 35.

It is noted that no constraints exist on the values of the angular displacement ϑ_{sk} ($k=1,...,n_a$) of each set from the α-axis. Therefore, each of the above configurations may be neither symmetrical nor asymmetrical. This aspect is a significant advantage over the VSD modeling. Consequently, the A-DMS modeling can deal with off-the-shelf stator cores designed for three-phase motors and unsuitable for the VSD modeling, thus reducing cost and design times [42].

$$[T_F] = \frac{1}{n_a} \cdot \begin{bmatrix} [T_{C,1}] & [T_{C,2}] & [T_{C,3}] & \cdots & [T_{C,n_a-2}] & [T_{C,n_a-1}] & [T_{C,n_a}] \\ w_1 \cdot [T_{C,1}] & q_1 \cdot [T_{C,2}] & q_1 \cdot [T_{C,3}] & \cdots & q_1 \cdot [T_{C,n_a-2}] & q_1 \cdot [T_{C,n_a-1}] & q_1 \cdot [T_{C,n_a}] \\ 0_{2\times3} & w_2 \cdot [T_{C,2}] & q_2 \cdot [T_{C,3}] & \cdots & q_2 \cdot [T_{C,n_a-2}] & q_2 \cdot [T_{C,n_a-1}] & q_2 \cdot [T_{C,n_a}] \\ 0_{2\times3} & 0_{2\times3} & w_3 \cdot [T_{C,3}] & \cdots & q_3 \cdot [T_{C,n_a-2}] & q_3 \cdot [T_{C,n_a-1}] & q_3 \cdot [T_{C,n_a}] \\ \cdots & \cdots & \cdots & \cdots & \cdots & \cdots & \cdots \\ 0_{2\times3} & 0_{2\times3} & 0_{2\times3} & \cdots & w_{n_a-2} \cdot [T_{C,n_a-2}] & q_{n_a-2} \cdot [T_{C,n_a-1}] & q_{n_a-2} \cdot [T_{C,n_a}] \\ 0_{2\times3} & 0_{2\times3} & 0_{2\times3} & \cdots & 0_{2\times3} & w_{n_a-1} \cdot [T_{C,n_a-1}] & q_{n_a-1} \cdot [T_{C,n_a}] \end{bmatrix}$$

(27)
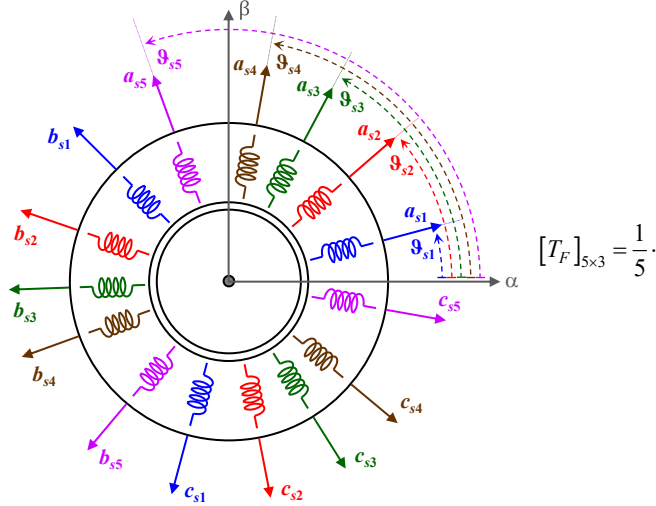
$$[T_F]_{5\times3} = \frac{1}{5} \cdot \begin{bmatrix} [T_{C,1}] & [T_{C,2}] & [T_{C,3}] & [T_{C,4}] & [T_{C,5}] \\ 2 \cdot [T_{C,1}] & -\frac{1}{2} \cdot [T_{C,2}] & -\frac{1}{2} \cdot [T_{C,3}] & -\frac{1}{2} \cdot [T_{C,4}] & -\frac{1}{2} \cdot [T_{C,5}] \\ 0_{2\times3} & \frac{\sqrt{15}}{2} \cdot [T_{C,2}] & -\sqrt{\frac{5}{12}} \cdot [T_{C,3}] & -\sqrt{\frac{5}{12}} \cdot [T_{C,4}] & -\sqrt{\frac{5}{12}} \cdot [T_{C,5}] \\ 0_{2\times3} & 0_{2\times3} & \sqrt{\frac{10}{3}} \cdot [T_{C,3}] & -\sqrt{\frac{5}{6}} \cdot [T_{C,4}] & -\sqrt{\frac{5}{6}} \cdot [T_{C,5}] \\ 0_{2\times3} & 0_{2\times3} & 0_{2\times3} & \sqrt{\frac{5}{2}} \cdot [T_{C,4}] & -\sqrt{\frac{5}{2}} \cdot [T_{C,5}] \end{bmatrix}$$

Fig. 32. A-DMS-based full-order matrix transformation for a generic penta-three-phase winding configuration (15-phase as 5·3-phase).
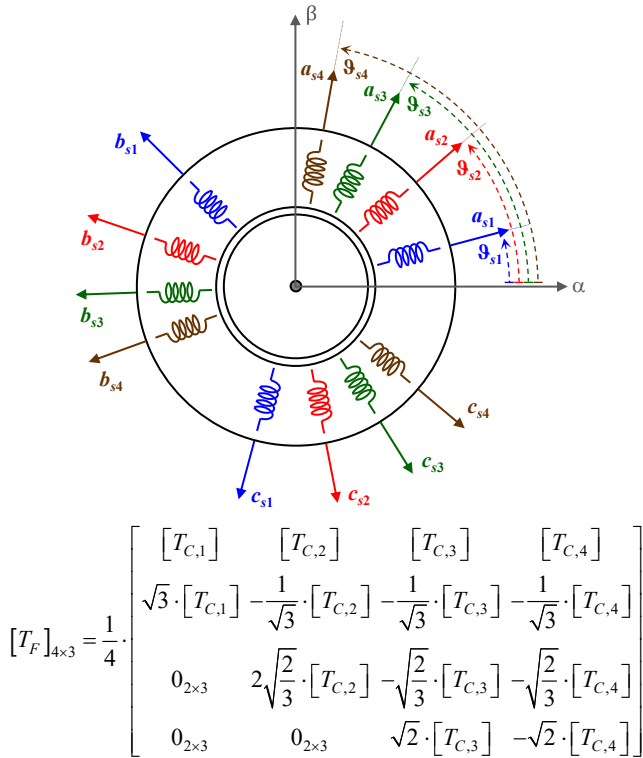
$$[T_F]_{4\times3} = \frac{1}{4} \cdot \begin{bmatrix} [T_{C,1}] & [T_{C,2}] & [T_{C,3}] & [T_{C,4}] \\ \sqrt{3} \cdot [T_{C,1}] & -\frac{1}{\sqrt{3}} \cdot [T_{C,2}] & -\frac{1}{\sqrt{3}} \cdot [T_{C,3}] & -\frac{1}{\sqrt{3}} \cdot [T_{C,4}] \\ 0_{2\times3} & 2\sqrt{\frac{2}{3}} \cdot [T_{C,2}] & -\sqrt{\frac{2}{3}} \cdot [T_{C,3}] & -\sqrt{\frac{2}{3}} \cdot [T_{C,4}] \\ 0_{2\times3} & 0_{2\times3} & \sqrt{2} \cdot [T_{C,3}] & -\sqrt{2} \cdot [T_{C,4}] \end{bmatrix}$$

Fig. 33. A-DMS-based full-order matrix transformation for a generic quad-three-phase winding configuration (12-phase as 4·3-phase).
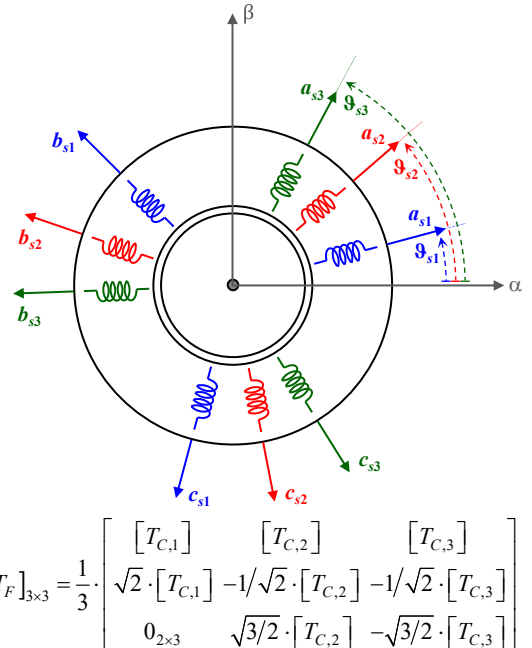
$$[T_F]_{3\times3} = \frac{1}{3} \cdot \begin{bmatrix} [T_{C,1}] & [T_{C,2}] & [T_{C,3}] \\ \sqrt{2} \cdot [T_{C,1}] & -1/\sqrt{2} \cdot [T_{C,2}] & -1/\sqrt{2} \cdot [T_{C,3}] \\ 0_{2\times3} & \sqrt{3/2} \cdot [T_{C,2}] & -\sqrt{3/2} \cdot [T_{C,3}] \end{bmatrix}$$

Fig. 34. A-DMS-based full-order matrix transformation for a generic triple-three-phase winding configuration (9-phase as 3·3-phase).
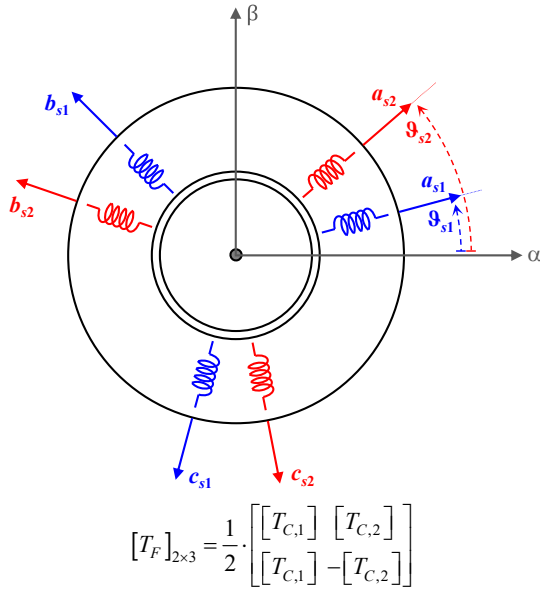
$$[T_F]_{2\times3} = \frac{1}{2} \cdot \begin{bmatrix} [T_{C,1}] & [T_{C,2}] \\ [T_{C,1}] & -[T_{C,2}] \end{bmatrix}$$

Fig. 35. A-DMS-based full-order matrix transformation for a generic dual-three-phase winding configuration (6-phase as 2·3-phase).

REFERENCES

[1] R. Bojoi, S. Rubino, A. Tenconi, and S. Vaschetto, 'Multiphase electrical machines and drives: A viable solution for energy generation and transportation electrification', in *2016 International Conference and Exposition on Electrical and Power Engineering (EPE)*, Oct. 2016, pp. 632–639. doi: 10.1109/ICEPE.2016.7781416.

[2] W. Cao, B. C. Mecrow, G. J. Atkinson, J. W. Bennett, and D. J. Atkinson, 'Overview of Electric Motor Technologies Used for More Electric Aircraft (MEA)', *IEEE Trans. Ind. Electron.*, vol. 59, no. 9, pp. 3523–3531, Sep. 2012, doi: 10.1109/TIE.2011.2165453.

[3] E. Levi, 'Multiphase Electric Machines for Variable-Speed Applications', *IEEE Trans. Ind. Electron.*, vol. 55, no. 5, pp. 1893–1909, May 2008, doi: 10.1109/TIE.2008.918488.

[4] A. Salem and M. Narimani, 'A Review on Multiphase Drives for Automotive Traction Applications', *IEEE Trans. Transp. Electrification*, vol. 5, no. 4, pp. 1329–1348, Dec. 2019, doi: 10.1109/TTE.2019.2956355.

[5] F. Barrero and M. J. Duran, 'Recent Advances in the Design, Modeling, and Control of Multiphase Machines—Part I', *IEEE Trans. Ind. Electron.*, vol. 63, no. 1, pp. 449–458, Jan. 2016, doi: 10.1109/TIE.2015.2447733.

[6] M. J. Duran and F. Barrero, 'Recent Advances in the Design, Modeling, and Control of Multiphase Machines—Part II', *IEEE Trans. Ind. Electron.*, vol. 63, no. 1, pp. 459–468, Jan. 2016, doi: 10.1109/TIE.2015.2448211.

[7] S. Rubino, I. R. Bojoi, F. Mandrile, and E. Armando, 'Modular Stator Flux and Torque Control of Multi-Three-Phase Induction Motor Drives', *IEEE Trans. Ind. Appl.*, vol. 56, no. 6, pp. 6507–6525, Nov. 2020, doi: 10.1109/TIA.2020.3022338.

[8] I. Zoric, M. Jones, and E. Levi, 'Arbitrary Power Sharing Among Three-Phase Winding Sets of Multiphase Machines', *IEEE Trans. Ind. Electron.*, vol. 65, no. 2, pp. 1128–1139, Feb. 2018, doi: 10.1109/TIE.2017.2733468.

[9] I. Zoric, M. Jones, and E. Levi, 'Voltage balancing control of a symmetrical nine-phase machine with series-connected DC links', in *2017 IEEE 26th International Symposium on Industrial Electronics (ISIE)*, Jun. 2017, pp. 1052–1057. doi: 10.1109/ISIE.2017.8001391.

[10] A. Tessarolo, G. Zocco, and C. Tonello, 'Design and Testing of a 45-MW 100-Hz Quadruple-Star Synchronous Motor for a Liquefied Natural Gas Turbo-Compressor Drive', *IEEE Trans. Ind. Appl.*, vol. 47, no. 3, pp. 1210–1219, May 2011, doi: 10.1109/TIA.2011.2126036.

[11] Y. Zhao and T. A. Lipo, 'Space vector PWM control of dual three-phase induction machine using vector space decomposition', *IEEE Trans. Ind. Appl.*, vol. 31, no. 5, pp. 1100–1109, Sep. 1995, doi: 10.1109/28.464525.

[12] E. Levi, R. Bojoi, F. Profumo, H. A. Toliyat, and S. Williamson, 'Multiphase induction motor drives - a technology status review', *IET Electr. Power Appl.*, vol. 1, no. 4, pp. 489–516, Jul. 2007, doi: 10.1049/iet-epa:20060342.

[13] P. Krause, O. Wasynczuk, S. D. Sudhoff, and S. Pekarek, *Analysis of Electric Machinery and Drive Systems*. John Wiley & Sons, 2013.

[14] I. Zoric, M. Jones, and E. Levi, 'Vector space decomposition algorithm for asymmetrical multiphase machines', in *2017 International Symposium on Power Electronics (Ee)*, Oct. 2017, pp. 1–6. doi: 10.1109/PEE.2017.8171682.

[15] M. Slunjski, O. Dordevic, M. Jones, and E. Levi, 'Symmetrical/Asymmetrical Winding Reconfiguration in Multiphase Machines', *IEEE Access*, vol. 8, pp. 12835–12844, 2020, doi: 10.1109/ACCESS.2020.2965652.

[16] G. Sala, M. Mengoni, G. Rizzoli, M. Degano, L. Zarri, and A. Tani, 'Impact of Star Connection Layouts on the Control of Multiphase Induction Motor Drives Under Open-Phase Fault', *IEEE Trans. Power Electron.*, vol. 36, no. 4, pp. 3717–3726, Apr. 2021, doi: 10.1109/TPEL.2020.3024205.

[17] W. N. W. A. Munim, M. J. Duran, H. S. Che, M. Bermúdez, I. González-Prieto, and N. A. Rahim, 'A Unified Analysis of the Fault Tolerance Capability in Six-Phase Induction Motor Drives', *IEEE Trans. Power Electron.*, vol. 32, no. 10, pp. 7824–7836, Oct. 2017, doi: 10.1109/TPEL.2016.2632118.

[18] I. G. Prieto, M. J. Duran, P. Garcia-Entrambasaguas, and M. Bermudez, 'Field-Oriented Control of Multiphase Drives With Passive Fault Tolerance', *IEEE Trans. Ind. Electron.*, vol. 67, no. 9, pp. 7228–7238, Sep. 2020, doi: 10.1109/TIE.2019.2944056.

[19] A. Tani, M. Mengoni, L. Zarri, G. Serra, and D. Casadei, 'Control of Multiphase Induction Motors With an Odd Number of Phases Under Open-Circuit Phase Faults', *IEEE Trans. Power Electron.*, vol. 27, no. 2, pp. 565–577, Feb. 2012, doi: 10.1109/TPEL.2011.2140334.

[20] R. H. Nelson and P. C. Krause, 'Induction Machine Analysis for Arbitrary Displacement Between Multiple Winding Sets', *IEEE Trans. Power Appar. Syst.*, vol. PAS-93, no. 3, pp. 841–848, May 1974, doi: 10.1109/TPAS.1974.293983.

[21] S. Rubino, O. Dordevic, R. Bojoi, and E. Levi, 'Modular Vector Control of Multi-Three-Phase Permanent Magnet Synchronous Motors', *IEEE Trans. Ind. Electron.*, vol. 68, no. 10, pp. 9136–9147, Oct. 2021, doi: 10.1109/TIE.2020.3026271.

[22] A. Galassini, A. Costabeber, M. Degano, C. Gerada, A. Tessarolo, and R. Menis, 'Enhanced Power Sharing Transient With Droop Controllers for Multithree-Phase Synchronous Electrical Machines', *IEEE Trans. Ind. Electron.*, vol. 66, no. 7, pp. 5600–5610, Jul. 2019, doi: 10.1109/TIE.2018.2868029.

[23] S. Rubino, R. Bojoi, E. Levi, and O. Dordevic, 'Vector Control of Multiple Three-Phase Permanent Magnet Motor Drives', in *IECON 2018 - 44th Annual Conference of the IEEE Industrial Electronics Society*, Oct. 2018, pp. 5866–5871. doi: 10.1109/IECON.2018.8591146.

[24] Y. Hu, Z. Q. Zhu, and M. Odavic, 'Comparison of Two-Individual Current Control and Vector Space Decomposition Control for Dual Three-Phase PMSM', *IEEE Trans. Ind. Appl.*, vol. 53, no. 5, pp. 4483–4492, Sep. 2017, doi: 10.1109/TIA.2017.2703682.

[25] J. Karttunen, S. Kallio, P. Peltoniemi, P. Silventoinen, and O. Pyrhönen, 'Decoupled Vector Control Scheme for Dual Three-Phase Permanent Magnet Synchronous Machines', *IEEE Trans. Ind. Electron.*, vol. 61, no. 5, pp. 2185–2196, May 2014, doi: 10.1109/TIE.2013.2270219.

[26] M. Zabaleta, E. Levi, and M. Jones, 'Modelling approaches for triple three-phase permanent magnet machines', in *2016 XXII International Conference on Electrical Machines (ICEM)*, Sep. 2016, pp. 466–472. doi: 10.1109/ICELMACH.2016.7732567.

[27] S. Rubino, R. Bojoi, D. Cittanti, and L. Zarri, 'Decoupled and Modular Torque Control of Multi-Three-Phase Induction Motor Drives', *IEEE Trans. Ind. Appl.*, vol. 56, no. 4, pp. 3831–3845, 2020, doi: 10.1109/TIA.2020.2991122.

[28] S. Rubino, O. Dordevic, E. Armando, I. R. Bojoi, and E. Levi, 'A Novel Matrix Transformation for Decoupled Control of Modular Multiphase PMSM Drives', *IEEE Trans. Power Electron.*, vol. 36, no. 7, pp. 8088–8101, Jul. 2021, doi: 10.1109/TPEL.2020.3043083.

[29] G. Pellegrino, R. I. Bojoi, and P. Guglielmi, 'Unified Direct-Flux Vector Control for AC Motor Drives', *IEEE Trans. Ind. Appl.*, vol. 47, no. 5, pp. 2093–2102, Sep. 2011, doi: 10.1109/TIA.2011.2161532.

[30] S. Rubino, E. Armando, R. Bojoi, and L. Zarri, 'Fault-Tolerant Torque Control Based on Common and Differential Mode Modeling for Multi-Three-Phase Induction Machines', in *2021 IEEE International Electric Machines Drives Conference (IEMDC)*, May 2021, pp. 1–8. doi: 10.1109/IEMDC47953.2021.9449509.

[31] M. Slunjski, O. Stiscia, M. Jones, and E. Levi, 'General Torque Enhancement Approach for a Nine-Phase Surface PMSM With Built-

In Fault Tolerance', *IEEE Trans. Ind. Electron.*, vol. 68, no. 8, pp. 6412–6423, Aug. 2021, doi: 10.1109/TIE.2020.3007053.

[32] R. Kianinezhad, B. Nahid-Mobarakeh, L. Baghli, F. Betin, and Gé.-A. Capolino, 'Modeling and Control of Six-Phase Symmetrical Induction Machine Under Fault Condition Due to Open Phases', *IEEE Trans. Ind. Electron.*, vol. 55, no. 5, pp. 1966–1977, May 2008, doi: 10.1109/TIE.2008.918479.

[33] I. R. Bojoi, E. Armando, G. Pellegrino, and S. G. Rosu, 'Self-commissioning of inverter nonlinear effects in AC drives', in *2012 IEEE International Energy Conference and Exhibition (ENERGYCON)*, Sep. 2012, pp. 213–218. doi: 10.1109/EnergyCon.2012.6347755.

[34] S. Rubino, R. Bojoi, M. Mengoni, and L. Zarri, 'Optimal flux selection for multi three-phase machines in normal and fault conditions', in *2017 IEEE International Electric Machines and Drives Conference (IEMDC)*, May 2017, pp. 1–8. doi: 10.1109/IEMDC.2017.8002313.

[35] Bon-Ho Bae, N. Patel, S. Schulz, and Seung-Ki Sul, 'New field weakening technique for high saliency interior permanent magnet motor', in *38th IAS Annual Meeting on Conference Record of the Industry Applications Conference, 2003.*, Oct. 2003, vol. 2, pp. 898–905 vol.2. doi: 10.1109/IAS.2003.1257641.

[36] A. M. Hava, R. J. Kerkman, and T. A. Lipo, 'Simple analytical and graphical methods for carrier-based PWM-VSI drives', *IEEE Trans. Power Electron.*, vol. 14, no. 1, pp. 49–61, Jan. 1999, doi: 10.1109/63.737592.

[37] M. S. A. Dahidah, G. Konstantinou, and V. G. Agelidis, 'A Review of Multilevel Selective Harmonic Elimination PWM: Formulations, Solving Algorithms, Implementation and Applications', *IEEE Trans. Power Electron.*, vol. 30, no. 8, pp. 4091–4106, Aug. 2015, doi: 10.1109/TPEL.2014.2355226.

[38] G. Rizzoli, G. Serra, P. Maggiore, and A. Tenconi, 'Optimized design of a multiphase induction machine for an open rotor aero-engine shaft-line-embedded starter/generator', in *IECON 2013 - 39th Annual Conference of the IEEE Industrial Electronics Society*, Nov. 2013, pp. 5203–5208. doi: 10.1109/IECON.2013.6699980.

[39] F. Mariut, S. Rosu, R. Bojoi, and A. Tenconi, 'Multiphase modular power converter using the PEBB concept and FPGA-based direct high speed voltage measurement', in *2015 17th European Conference on Power Electronics and Applications (EPE'15 ECCE-Europe)*, Sep. 2015, pp. 1–10. doi: 10.1109/EPE.2015.7309332.

[40] E. Jung, H. Yoo, S. Sul, H. Choi, and Y. Choi, 'A Nine-Phase Permanent-Magnet Motor Drive System for an Ultrahigh-Speed Elevator', *IEEE Trans. Ind. Appl.*, vol. 48, no. 3, pp. 987–995, May 2012, doi: 10.1109/TIA.2012.2190472.

[41] S.-H. Kim and S.-K. Sul, 'Maximum torque control of an induction machine in the field weakening region', *IEEE Trans. Ind. Appl.*, vol. 31, no. 4, pp. 787–794, Jul. 1995, doi: 10.1109/28.395288.

[42] A. S. Abdel-Khalik, A. M. Massoud, and S. Ahmed, 'Application of Standard Three-Phase Stator Frames in Prime Phase Order Multiphase Machine Construction', *IEEE Trans. Ind. Electron.*, vol. 66, no. 4, pp. 2506–2517, Apr. 2019, doi: 10.1109/TIE.2018.2840497.